Original draft writing: S.S.S., K., K.M., H.K.

Writing, review and editing: A.K.S., V.S., H.Y.N., D.V., V.K.T.

Supervision: S.S.S., V.K.T.

All authors have read and agreed to the published version of the manuscript.

Novel synthesis methods and applications of MXene-based nanomaterials (MBNs) for hazardous pollutants degradation: Future Perspectives

Samarjeet Singh Siwal [a*], Karamveer Sheoran [a], Kirti Mishra [a], Harjot Kaur [a], Adesh Kumar Saini [b], Vipin Saini [c], Dai-Viet N. Vo [d], Hamed Yazdani Nezhad[e], and Vijay Kumar Thakur [f,g*]

[a] Department of Chemistry, M.M. Engineering College, Maharishi Markandeshwar (Deemed to be University), Mullana-Ambala, Haryana, 133207, India

[b] Department of Biotechnology, M.M. Engineering College, Maharishi Markandeshwar (Deemed to be University), Mullana-Ambala, Haryana, 133207, India

[c] Department of Pharmacy, Maharishi Markandeshwar University, Kumarhatti, Solan, Himachal Pradesh, 173229, India

[d] Center of Excellence for Green Energy and Environmental Nanomaterials (CE@GrEEN), Nguyen Tat Thanh University, Ho Chi Minh City, Vietnam

[e] Department of Mechanical Engineering and Aeronautics, City University of London, London EC1V0HB, UK

[f] Biorefining and Advanced Materials Research Center, SRUC, Edinburgh EH9 3JG, UK

[g]School of Engineering, University of Petroleum & Energy Studies (UPES), Dehradun, Uttarakhand, India

*Corresponding authors: samarjeet6j1@gmail.com (Samarjeet Singh Siwal), Vijay.Thakur@sruc.ac.uk (Vijay Kumar Thakur)

Abstract:

MXenes are a quickly growing and extended group of two-dimensional (2D) substances that have earned unbelievable analysis credits for various application areas within different manufacturing areas. Due to novel essential architectural and physicochemical properties shows good properties, such as elevated exterior area, living adaptability, strong electrochemistry, and great hydrophilicity. Given the fast progress within the structure and synthesis of MBNs for water treatment, quick updates on this research field are required to remove toxic substances, such as production approaches and characterization methods for the advantages and constraints of MXenes for pollutant degradation. MXenes are

determined as a proposed road toward atmosphere-clean-up machinery to identify and decrease a pattern of hazardous resistant pollutants from environmental forms. Here, in this review article, we have been focused on describing the overview, novel synthesis methods, and characteristics of the MXene-based nanomaterials (MBNs) in the field for removing hazardous contaminants from environmental conditions. In the last, the utilizations of MBNs in water sanitization, organic solvent filtration, antibiotics degradation, pesticide degradation, heavy metals degradation, ions removal, bacterial pathogens degradation, along with the conclusion, challenges, and prospects in this field, have been discussed.

Keywords: *MXene-based nanomaterials; electrical properties; water purification; pesticide degradation; bacterial pathogens degradation.*

Graphical abstract:

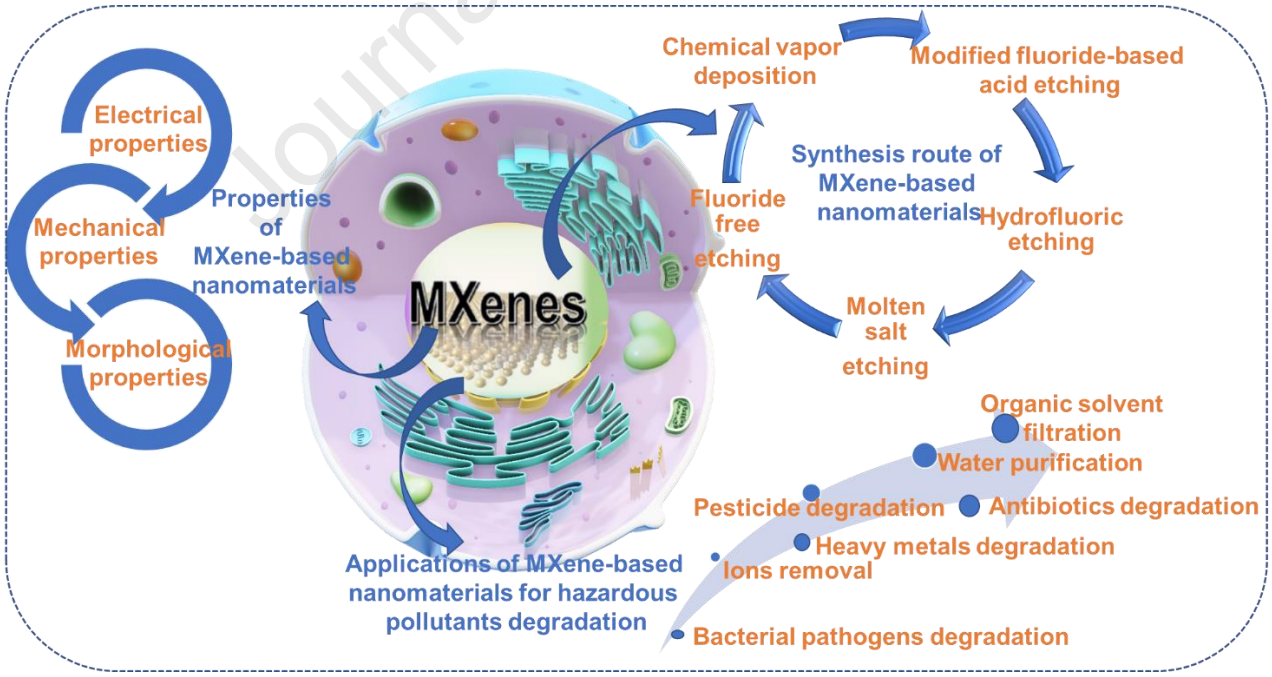

Abbreviations:

2D	*Two-dimensional*
TMCs	*Transition metal carbides*
MBNs	*MXene-based nanomaterials*
TM	*Transition metal*
Gr	*Graphene*
CNTs	*Carbon nanotubes*
MOFs	*Metal-organic frameworks*
Ti_4N_3	*Titanium nitride*
TBAOH	*Tetrabutylammonium hydroxide*
XRD	*X-ray diffraction*
CVD	*Chemical vapour deposition*
CH_4	*Methane*
SEM	*Scanning electron microscopy*
WFs	*Work finctions*
TEM	*Transmission electron microscopy*
DMSO	*Dimethyl sulfoxide*
QDs	*Quantum dots*
PEI	*Polyethyleneimine*
3D	*Three-dimensional*
GO	*Graphene oxide*
RhB	*Rhodamine B*
MB	*Methyl blue*
MO	*Methyl orange*

4-NA	*4-nitroanilne*
h-BN	*Hexagonal boron nitride*
LDHs	*Layered double hydroxides*
gC_3N_4	*Graphitic carbon nitride*
AV	*Avermectin*
S. aureus	*Staphylococcus aureus*
E. coli	*Escherichia coli*
H&E	*Hematoxylin and eosin*
HF	*Hydrofluoric acid*
PDSs	*Pesticide delivery systems*
CAs	*Contrast agents*
ROS	*Reactive oxygen species*
MBNs	*MXene-based nanomaterials*

1. Introduction

To minimize the environmental impact, the advancement of the latest developing nanomaterials and polymers in particular for dangerous pollutants degradation has brought more innumerable attention recently (Ashvinder K. Rana et al., 2021a, 2021b; Ashvinder Kumar Rana et al., 2021; Siwal et al., 2021; Usmani et al., 2020). MXenes is a general name for a group of new two-dimensional (2D) transition metal carbides (TMCs) and carbonitrides substances with graphene-similar arrangements (Siwal et al., 2020a; Siwal et al., 2020b). Being a novel class of 2D lamellar nanocomposite, various researchers have concentrated on designing and synthesizing MBNs due to their sizeable inter-layer annulled by the 2D loading arrangement and a high surface area rich adaptable surface functional group, and great hydrophilicity. Regarding their unusual characteristics, relevant analysis and latent of 2D MXenes nanocomposite for pollutants parting and water processing purposes are implemented (Li et al., 2021a; Li et al., 2021c; Wang et al., 2021).

MXenes is a novel, and a large group of 2D elements that occur below initial TMCs and carbonitrides have earned particular investigation concerns in current years (Siwal et al., 2018). Due to their different architectural, physical, chemical, and practical properties, MXenes are recognized as architect nanomaterials for several manufacturing utilization e.g., water purification (such as; flux and removal) and organic solvent filtration (Al-Hamadani et al., 2020). The accelerated progress during global industrialization has proposed strict environmental attention (Shao and Chen, 2013; Jasper et al., 2017). At this point, the liberation of industrial scrap in the absence of the usual method is one of the main reasons for ecological contamination. The high volume of polluted effluent comprises a blend of toxic azo colorants, insecticides, and heavy metals of different applications

associated with coloring, printing, plastics, leather, diet, and drugs (Robinson et al., 2001; Islam et al., 2021; Rathi et al., 2021; Siwal et al., 2021b; Siwal et al., 2021c). In broad, ecological contaminants would be categorized as biological and inorganic, while poisonous heavy metals and colorants are the prime causes of water pollution(Sharma et al., 2020; Thakur et al., 2022, 2018; Verma et al., 2020).

Also, MXenes have a typical description of $M_{n+1}X_nT_x$, while "M" indicates a transition metal (TM), "X" may be a carbon (C)/nitride (N), n = 1∼3, and T_x denotes the related exterior functionalities (similar to -OH, -F and -O) (Siwal et al., 2019b; Xu and Gogotsi, 2020; Zhu et al., 2021). These exterior functionalities have a meaningful connection toward the physical and chemical characteristics of MXene substances that will further impact their latent within surface-cooperative utilization, for example, adsorption or film separation. MXenes give higher hydrophilicity and performance to ion exchange and oxidation-reduction owing to their surface functionalities with different graphene (Gr), such as lower hydrophilicity. Besides, the 2D composition, united by solid redox property, has identified MXenes' potential to manufacture photocatalyst and electrocatalytic devices toward the degeneration and signal of ecological pollutants (Schultz et al., 2019; Kumar et al., 2022; Rasheed et al., 2022). The accelerated evolution of MXenes into environmental remedy and discovery machinery asks for an impartial conclusion of the importance of their surface relevant characteristics upon the conclusive activity of MXene-dependent composites (Tunesi et al., 2021). Young-Kyu and his coworkers (Ranjith et al., 2021; Ranjith et al., 2022) based their studies on 1D-2D MBNs as a better-performance electrochemical detection stage toward the sensitive recognition of dihydroxybenzene isomers and rutin within wastewater specimens.

Here, in our study we have tried to summarize all the insight view on history, synthesis routes of MBNs and all the possible aspects in this regard. As per our knowledge this is first review where readers can go through overview of novel synthesis methods, and characteristics of the MXene-based nanomaterials (MBNs) in the field for removing hazardous contaminants from environmental conditions. In the last, the utilizations of MBNs in water sanitization, organic solvent filtration, antibiotics degradation, pesticide degradation, heavy metals degradation, ions removal, bacterial pathogens degradation and other applications (such as, biosensing, biosafety, therapy, antimicrobial and diagnostic imaging), along with the conclusion, the existing challenges, and future direction in this field, have been discussed.

2. History and overview of MXene-based nanomaterials

Hexagonal panel structured ternary TMCs or nitrides, including the architectural description of $M_{n+1}AX_n$ has been identified as a MAX segment (Barsoum and Radovic, 2011; Sun, 2011). At this juncture, M is the initial TM (Such as Ti, Cr, V, Mo, Zr, Nb, Sc and W), where X is the C and/or N, while A is the enclosed component of covered $M_{n+1}X_n$, that is chosen by 13 or 14 groups within the periodic table (Naguib et al., 2011; Anasori et al., 2017). Expressly, “n” may be changed from 1 to 3. Therefore, the MAX segment is especially possible within the 413, 312, and 211 arrangements. The 312 (Ti_3AlC_2) assembly was identified as a generally studied MXene arrangement. **Fig. 1** shows the MAX stage elements and the attainable 413, 312, and 211 MAX segment configurations. See that the M-X tie is chemically durable associated with the M-A connection within the $M_{n+1}AX_n$. Therefore, “A” elements are very chemically in heat or etching methods (Sreedhar and Noh,

2021). Furthermore, the M-A connection is metallic. Hence, the MAX phase shows novel thermal and electrically conductive characteristics.

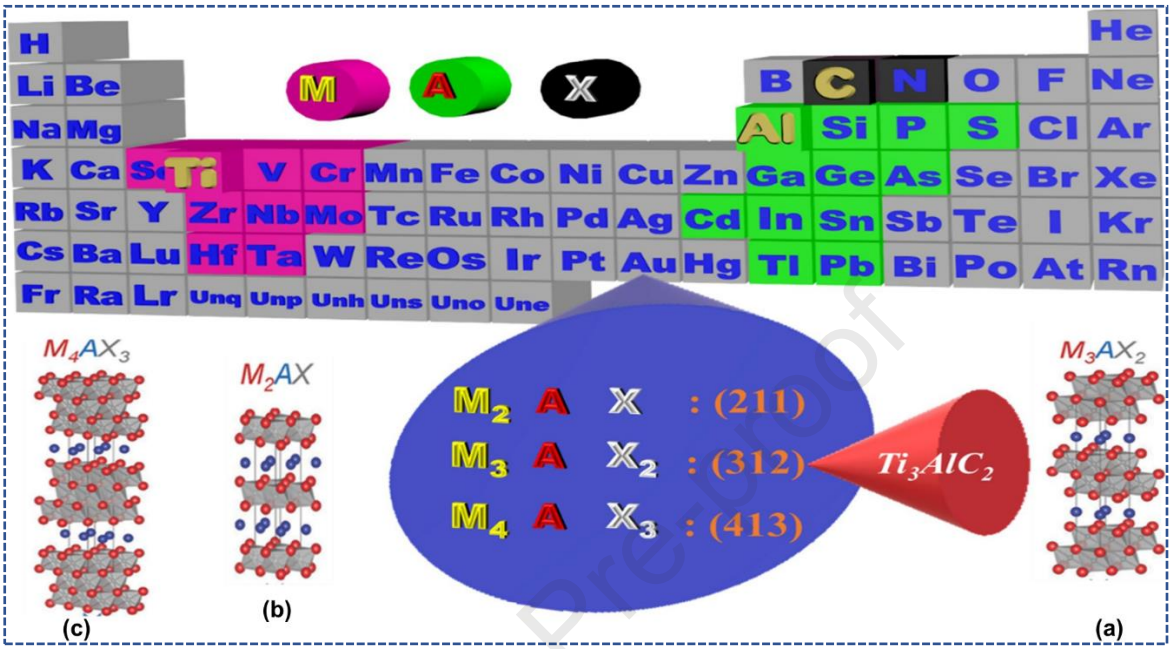

Fig. 1. The probable MAX segment components within the periodic table by (a) (3 1 2) (b) (2 1 1), and (c) (4 1 3) MAX stage element compartments. Reprinted with permission from Ref. (Sreedhar and Noh, 2021).

Various new researches have studied the construction of multi-faceted MXene flakes and nanocomposites (Anasori et al., 2017) through wet etching with HF (Ren et al., 2016), HCl-LiF (Chen et al., 2018; Couly et al., 2018), or HCl-NaF (Liu et al., 2017a). **Fig. 2** displays a timeframe of MXene incorporation since 2011 to 2019 (Al-Hamadani et al., 2020). Generally, nanomaterial-based films, which comprise carbon nanotubes (CNTs) (Siwal et al., 2021a), graphene oxides (GO) (Samarjeet et al., 2017; Siwal et al., 2019a), and/or metal-organic frameworks (MOFs), there are three invention techniques toward films:

1. MXenes are utilized as support substances toward the invention of a lamellar composition.

2. Various extracts or other nanomaterials are combined to incorporate composite medium films beside MXenes.
3. MXenes are used as covering substances to transform a membrane backing sheet.

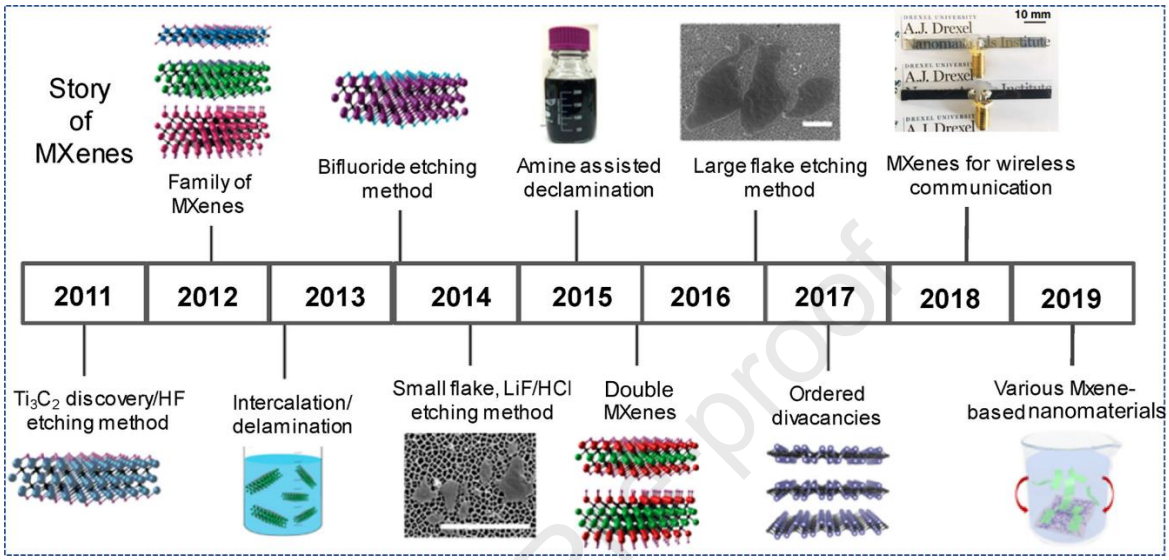

Fig. 2. Timeframe of MXenes: after Ti_3C_2 discovery to methodical divacancies adapted from Ref. (Al-Hamadani et al., 2020).

After 2011, numerous research articles (**Fig. 3**) and a book were proclaimed, and many licenses were registered based MBNs. In this regard, Naguib *et al.* (Naguib et al., 2021) reviewed significantly than the number of patents registered and allotted is the broad range of probable applications, varying from electronics to drug, sensing, communication, optoelectronics, and tribology between many other.

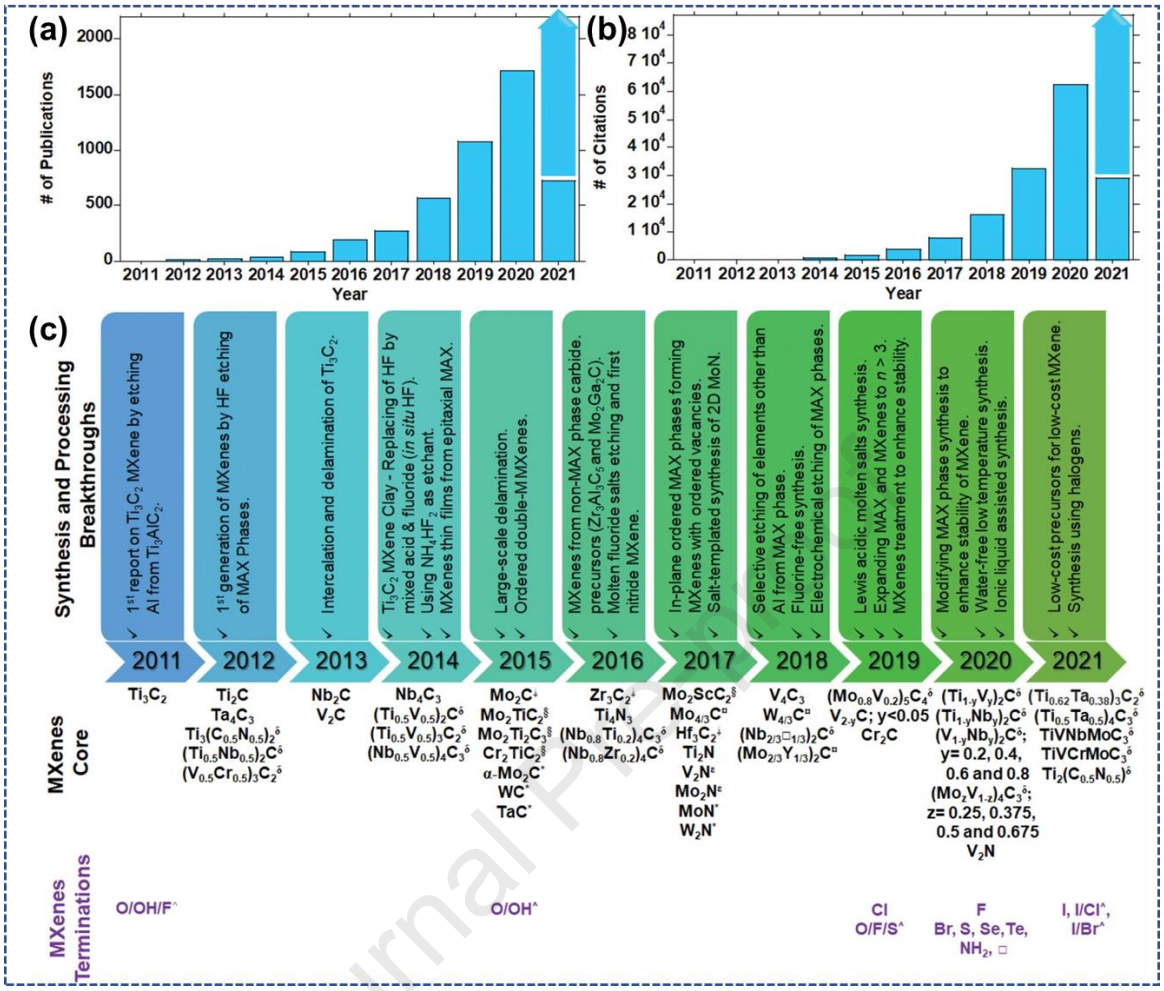

Fig. 3. Sequential displays of development within the area of MXenes. (a) The papers and (b) credentials data get by Web of Science. (c) Listing the direct integration and processing discoveries past the initial 10 years of MXenes' investigation. Reprinted with permission from Ref. (Naguib et al., 2021).

$^{\delta}$ Compact solution MXenes; $^{\square}$ MXene by non-MAX segment reactants; § out-of-plane well-organized dual TM MXene; $^{¤}$ MXene by in-plane well-organized dual TM MAX segment equivalents; * 2D carbides and nitrides shaped through bottom-up methods; $^{\varepsilon}$ nitride MXene shaped through post-processing of carbide MXene; $^{\square}$ position; and $^{\wedge}$ miscellaneous ends.

3. Synthesis route of MXene-based nanomaterials

There is a big group of triple carbides and nitrides MAX phases by fixed double TM constructions. The ball-milling and elevated heat sintering process makes MAX phases (Zhang et al., 2018b). Contrasting the amalgamation of Gr or MoS_2, MXenes are broadly formed through discerning etching of specific atomic films of their coated antecedents, like MAX phases. The mechanical depilation process is complicated because of the solid metallic interactions among the "A" and "M" elements into the MAX states. Though "M-A" bonds are further chemically dynamic compared to the more robust "M-X" interactions, therefore, it is probable to prepare a particular etching of "A" films to develop MAX phases. Extremely discerning etching is the critical requirement for building MXenes through remarkable operating techniques, for example, the HF approach (Wang et al., 2015; Zhang et al., 2015; Xiao et al., 2016), fluoride-comprising acid solution processing and heating (Horlait et al., 2016; Lukatskaya et al., 2017; Zhang et al., 2017). Following this profoundly selective etching, the compact MAX phase is changed to the sluggish accordion-similar MXene (Augustyn and Gogotsi, 2017). This unique etching of the "M-A" interaction in $M_{n+1}AX_n$ segments may be reviewed as given (Yang et al., 2019):

$$M_{n+1}AX_n + 3HF \rightarrow M_{n+1}X_n + AF_3 + \frac{3}{2}H_2 \quad \rightarrow \quad (1)$$

$$M_{n+1}X_n + 2H_2O \rightarrow M_{n+1}X_n(OH)_2 + H_2 \quad \rightarrow \quad (2)$$

$$M_{n+1}X_n + 2HF \rightarrow M_{n+1}X_nF_2 + H_2 \quad \rightarrow \quad (3)$$

Subsequent etching of the A sheet (1), the bulk of received $M_{n+1}X_n$ will proceed to combine by Water (2) and HF (3) to develop a functional group-comprising exterior. Furthermore, **Table 1** shows the different synthesis protocols of MBNs.

Table 1. Different synthesis protocols of MBNs.

Sr. No.	Types of MXene-based electrodes	Surface area (m^2g^{-1})	Cell voltage (V)	Salt adsorption capacity (mg/g)	Synthesis protocol	References
1	Ti_3C_2		1.2	13	HF	(Srimuk et al., 2016)
2	Ar plasma modified $Ti_3C_2T_x$		1.2	26.8	HF	(Guo et al., 2018)
3	Porous $Ti_3C_2T_x$		1.2	45	HF	(Bao et al., 2018)
4	LiF/HCL-etched $Ti_3C_2T_X$ MXene	2.1	1.2	68	LiF/HCL-etching process	(Ma et al., 2020)
5	Mn_3O_4/RGO nanoarchitectu-re	160	1.2	15	Hydrothermal synthesis method	(Bharath et al., 2020)
6	Ti_3C_2 MXene	6	1.2	13 ± 2	Traditional etching method	(Srimuk et al., 2016)

7	Porous $Ti_3C_2T_x$ MXene	293	1.2	45	Ti_2AlC ball milling	(Bao et al., 2018)
8	NTP/MXene (NTP/M) nanohybrid of Ti_3C_2 MXene	24.3	1.8	128.6	Lower electrical conductivity under solvothermal conditions	(Chen et al., 2021)

3.1. HF etching

Additionally, in the usual HF acid system, the A atom films may be discriminating extracted through MAX forms' elevated heat etching process (Urbankowski et al., 2016; Li et al., 2018b). Recently, Yang *et al.* (Yang et al., 2019) strongly built 2D titanium nitride (Ti_4N_3) utilizing the elevated-heat etching technique. **Fig. 4 (a)** Constructions of MAX states and similar MXenes and, In the improved method (**Fig. 4b**), they heated Ti_4AlN_3 in hot fluoride salt to select the Al element on 550 °C. The single or multi-faceted $Ti_4N_3T_x$ MXene was decorticated through the organic salt tetrabutylammonium hydroxide (TBAOH) method. As exhibited within **Fig. 4(d)**, the $Ti_4N_3T_x$ structure achieved through the elevated heat etching process has the identical organ-similar composition as HF etching. As recorded in **Fig. 4(c)**, (I), the Al removal method is limited by aluminium hydroxides under low-temperature circumstances. (II) Following high heat and low NaOH absorptions, the aluminium hydroxides $Al(OH)_3$ are slightly disappeared, but the $Ti_3C_2T_x$ is oxidated, and (III) elevated heat and higher NaOH absorptions will assist terminate the $Al(OH)_3$ and limit $Ti_3C_2T_x$ from essentially oxidated. As shown in **Fig. 4(e)**, the $Ti_3C_2T_x$ structure achieved applying 27.5 m NaOH below 270 °C has the identical organ-similar composition as through HF etching. It is clear about the $Ti_3C_2T_x$*;* if it were operated on 550 °C in the presence of an oxygen environment, it would be oxidized toward TiO_2 and oxides of C.

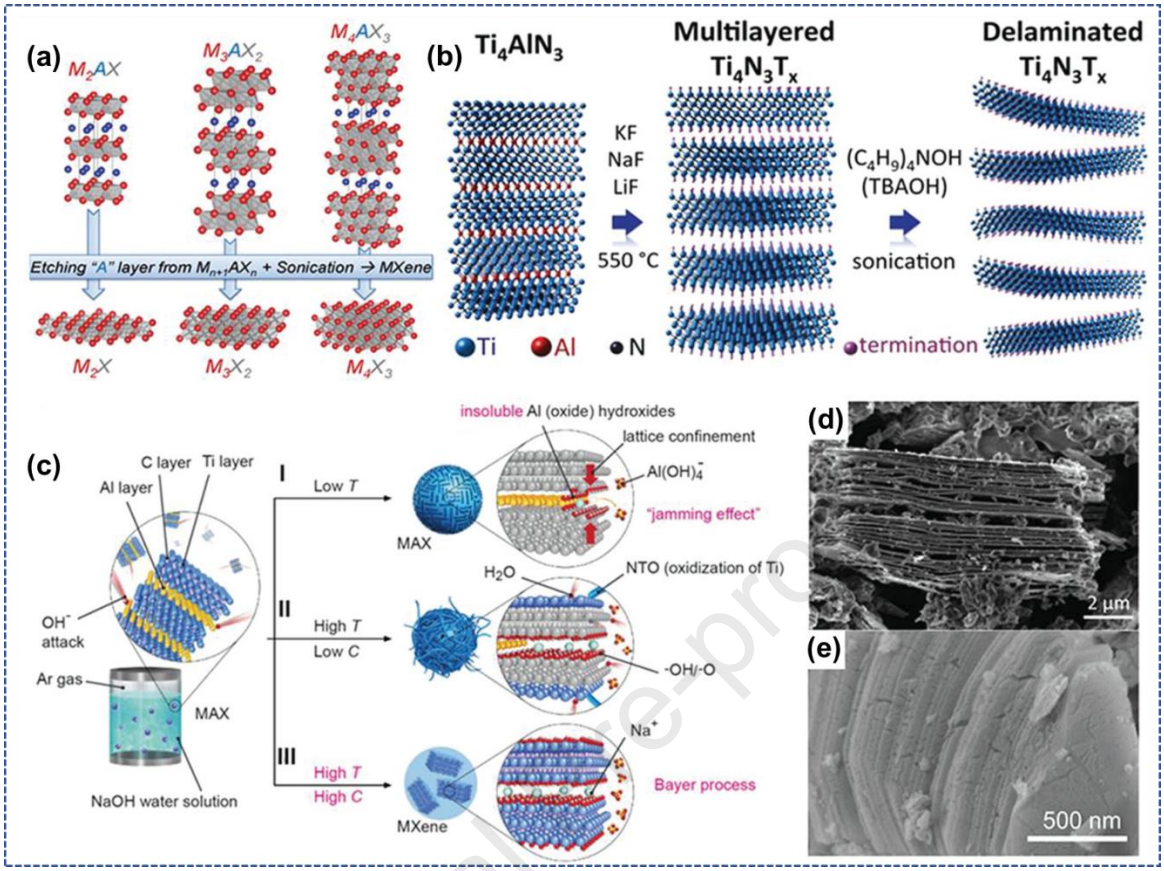

Fig. 4. **(a)** Structures of MAX states and similar MXenes. **(b)** Graphic of the construction of $Ti_4N_3T_x$ with heating below Ar, into molten salt at 550 °C. **(c)** Diagram of the reaction among Ti_3AlC_2 and NaOH below distinct situations. **(d)** SEM picture of $Ti_4N_3T_x$. **(e)** SEM picture of $Ti_3C_2T_x$ attained with 27.5 m NaOH below 270 °C. Reprinted with permission from Ref. (Yang et al., 2019).

Mostly, the outcomes afterwards HF etching are accordion-similar bits, preferably than the actual 2D substances. Solitary or multi-sheet MXene sheets can be achieved through sonication; though, the yield is restricted due to the solid communicating strength of the built MXene films. A kind of immense cations (Wang et al., 2016) or giant organic particles (Mashtalir et al., 2013; Osti et al., 2016) could be interpolated within multilayer MXene. compositions, growing the c-lattice constraint and reducing the synergy strengths among multi-layer MXenes sheets. Simultaneously, the interpolated multilayer MXenes may quickly be delaminated within water through staggering to make a steady colloidal

suspension holding of multilayer MXene flakes (Wang et al., 2017). This method changed and explained the aforementioned arduous embolism methods, permitted the larger-range generation of MXenes and supported this field's studies. **Fig. 5(a)** exhibits the architectural development from Ti_3AlC_2 to d-$Ti_3C_2T_x$, showing the removal of the Al from Ti_3AlC_2 and generation of 2D $Ti_3C_2T_x$, after the intercalation of LiOH in $Ti_3C_2T_x$ layers. **Fig. 5(b)** displays a representative SEM picture for the stacks of the new Ti_3C_2Tx multilayers. Later exfoliation through sonication into IPA by LiOH as intercalator, the d-Ti_3C_2Tx shows 2D flakes among few-layer coating upon silicon support (Fig. 4c), showing large Ti_3C_2Tx nanosheets may be readily incorporated through such liquid-phase moulting process. An AFM photograph further proves the delamination of $Ti_3C_2T_x$ from multilayer to few-layer in **Fig. 5(d)**. As explained under the corresponding height outline (**Fig. 5e**), the medium thickness of d-$Ti_3C_2T_x$ nanosheets is around 5 nm, corresponding to 3-4 sheets $Ti_3C_2T_x$, as the layer spacing with the *c*-axis is approximately 1.36 nm.

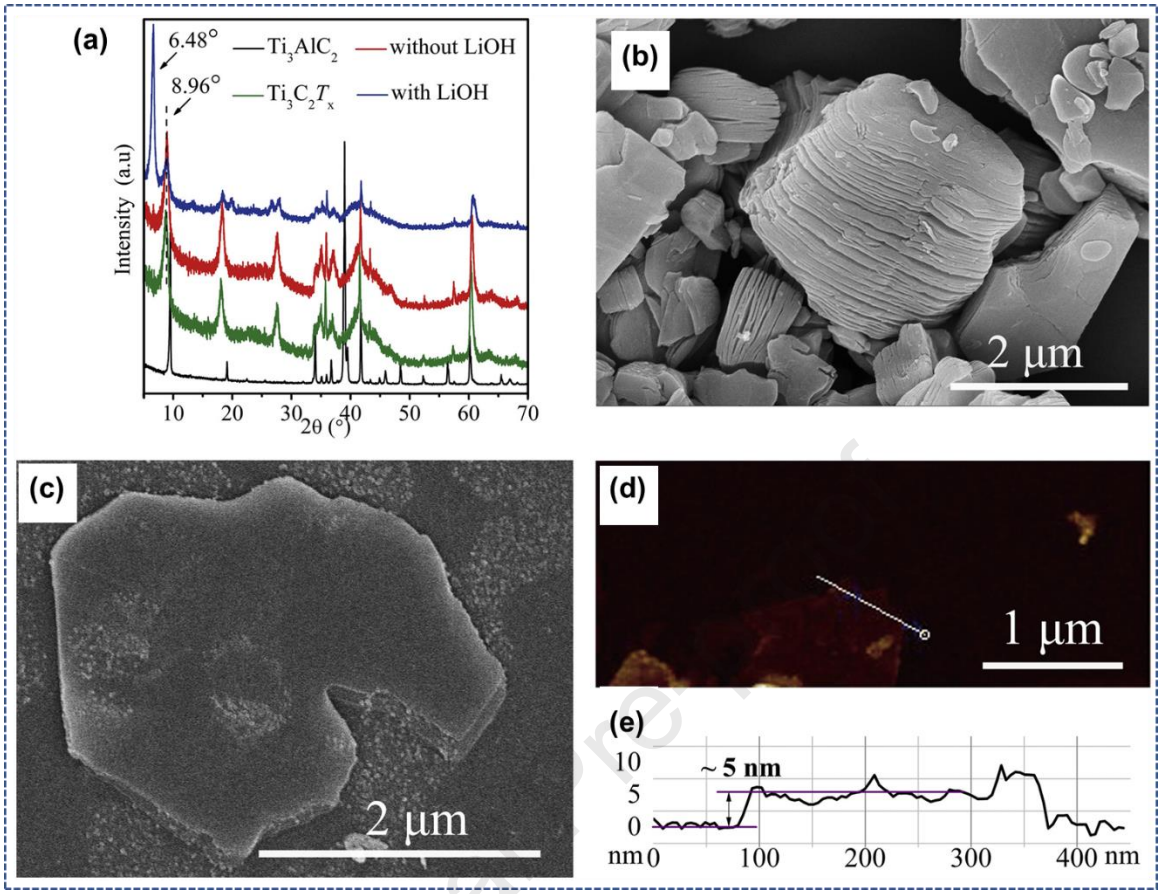

Fig. 5. (a) XRD spectra of the Ti_3AlC_2, the pure $Ti_3C_2T_x$ and ultrasonication flaked $Ti_3C_2T_x$ with and in the absence of LiOH in IPA; **(b)** SEM of the pure $Ti_3C_2T_x$; **(c)** SEM of the decorticate $Ti_3C_2T_x$; **(d)** AFM picture and **(e)** the similar line examination of the d-$Ti_3C_2T_x$ nanosheet on SiO_2/Si support. Reprinted with permission from Ref. (Wang et al., 2017).

3.2. Modified fluoride-based acid etching

To approach the high poisonousness connected by HF etching, scientists have completed numerous attempts to selectively investigate benign approaches to eliminate A atom films by MAX precursors. Besides HF, a hybrid suspension of a fluoride salt (e.g., LiF, NaF, KF, and NH_4F) and a great acid may also be utilized to etch MAX indications (Ghidiu et al., 2014). This is observed that fluoride salts and sturdy acids may act and develop facile HF to etch A atoms and start the embolism of positive ion selectively (for example, Li^+, Na^+, K^+, and NH_4^+) and water among MXene sheets through improving the interlayer layout of

MXene and reducing the synergy of MXene sheets. Remarkably, both the absorption of concentrated acid and fluoride salt may affect the character and dimension of the concluding MXene cells. The synthesized multilayered Ti_3C_2 generated through the clay process (5 M LiF/6 M HCl) requires additional sonication chosen delaminated within individual flakes, making incomplete and small MXene layers (Alhabeb et al., 2017).

3.3. Molten salts etching

As well as HF/fluoride-related acid etching, MXene may be formed by elevated heat processing of MAX forms, for example, employing Ti_4AlN_3 within a blend of molten fluoride salt 550°C below argon shield to give Ti_4N_3 (Urbankowski et al., 2016). The etching method may be made in a comparatively short time, about 30 minutes, because of the more profound durability of Ti_nN_{n-1} than the Ti_nC_{n-1}. Ti_nN_{n-1} may be dissociated while utilizing HF or fluoride-related acid as an etchant. Hence, a comparatively fast analysis time is the success of this heated salts etching process. Despite this, an extra wash method (through H_2SO_4 and DI water) and additional delamination (within TBAOH suspension) are essential.

The X-ray diffraction (XRD) analysis showed that the excorticate $Ti_4N_3T_m$ showed lower crystallinity than the other HF-etched $Ti_3C_2T_m$ (Alhabeb et al., 2017). It might recommend that there are still some problems synthesizing nitride MXenes via the melted fluoride salt etching process. Usually, the wet chemistry methods are yet the utmost suitable optimal for the amalgamation of MXene substances.

3.4. Fluoride-free etching

Though various etching situations have been established toward integrating MXenes, HF or fluoride-dependent composites are needed within most assembly techniques, which may prompt -F and -O termini upon the interface MXenes (Naguib et al., 2011). Remarkably, -F ends to harm the electrochemical activity of MXenes-based energy storage applications (Yu et al., 2019). Here, fluoride-free synthesis methods are required to develop a suitable electrochemical appearance. Zhang *et al*. (Li et al., 2018b) produced an alkali-supported hydrothermal etching technique to develop Ti_3C_2 MXene through utilizing NaOH solution as the etchant. Generally, for the Ti_3AlC_2 MAX phase, alkali is probably possible as an etchant owing to the significant connection between alkali and elemental Al. Usually, the Ti_3C_2 design is weak within the alkaline media, in that the deterioration of Ti_3C_2 design will coincide in the elimination of A atoms. Hence, retaining the Ti_3C_2 film unimpaired during the selective etching from Ti_3AlC_2 is a hurdle. Here, an elevated (270 °C), higher alkaline distillate (27.5 m) circumstance was utilized to stop the destruction of the Ti_3C_2 frame, that is recognized as the Bayer method.

Usually, the acquired MXenes are independent of -F ends when generated through the fluoride-free etching process. NaOH etching is less dangerous associated with HF and transformed fluoride-dependent acid etching but needs elevated heat and density of etchant (Bai et al., 2021; Song et al., 2021a). Furthermore, TMAOH etching is effective in excorticate; nonetheless, the captured $Al(OH)_4^-$ closes within MXenes can negatively affect their possible purposes.

3.5. Chemical vapour deposition

The “A” element may be assigned through an electrochemical approach. Although, this approach may not selectively remove the “A” film while grasping the “M” element. The

electrochemical method used to MAX phases could probably produce vague carbon. Hence, the yield acquired through this approach will not be an MXene. Behind the above-preparation processes, chemical vapour deposition (CVD) may instantly incorporate the 2D TMCs. In 2015, the crystalline α-Mo_2C was favorably manufactured with CVD with a super-tinny composition and extended range (Gogotsi, 2015; Xu et al., 2015; Liu et al., 2016b).

Aside from the as-mentioned etching techniques, CVD gives a possible path to manufacture superior MXene. During 2015, Ren's organization used a CVD technique to produce ultrathin α-Mo_2C 2D crystalline with an adjacent dimension of 100 μm through utilizing CH_4 as the carbon reservoir and double metallic foils (a Cu foil over a Mo foil) as the support (Xu et al., 2015). The CVD-developed MXene individual quartzes have larger sphere size and lower deficits than those manufactured through wet-chemical etching techniques. The CVD technique may be practiced to make different ultrathin TMC, for example, WC and TaC crystals. However, a limited article about the CVD assembly of MXene single layer shows that further advancement is still required. While the wet-chemistry etching process, CVD-developed MXene has a significantly lower concentration of deficiencies and disarrays and lower pollutants concentrations, allowing researchers to study the fundamental physical, chemical, electrical, and optical characteristics MXene. Lastly, the Scanning electron microscopy (SEM) pictures of powder surface structure taken through various etching techniques are displayed within **Fig. 6(a-j)** (Yu et al., 2019).

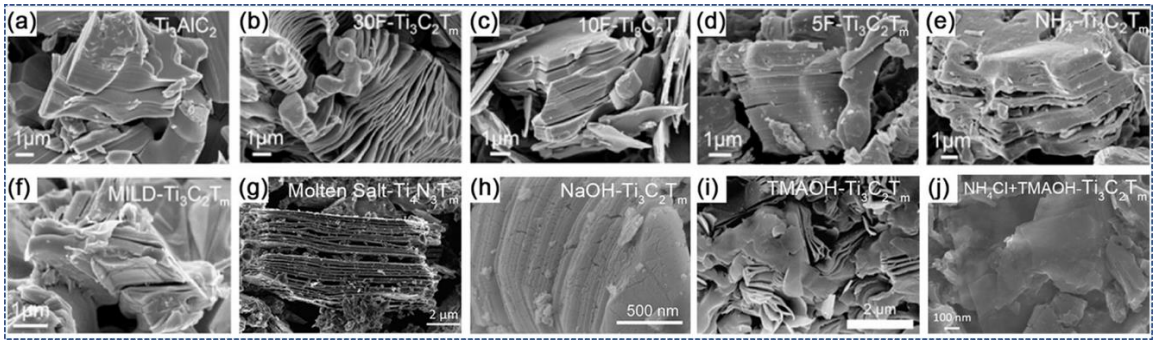

Fig. 6. SEM pictures of MBNs precipitates gained through diverse etching approaches. **(a)** Ti_3AlC_2 precipitate and multifaceted $Ti_3C_2T_m$ precipitate manufactured by **(b)** 30, **(c)** 10, and **(d)** 5 wt% HF. **(e)** Multi-faceted NH_4-$Ti_3C_2T_m$ precipitate made by NH_4F and HCl and **(f)** MILD-$Ti_3C_2T_m$ precipitate etched by 10 m LiF within 9 m HCl. **(g)** Molten salt preserved Ti_4AlN_3 at 550 °C for 0.5 h below Ar flow. **(h)** $Ti_3C_2T_m$ powder gained with 27.5 m NaOH below 270 °C. **(i)** $Ti_3C_2T_m$ precipitate got by aqueous TMAOH. **(j)** The electrochemical etched $Ti_3C_2T_m$ precipitate. Reprinted with permission from Ref. (Yu et al., 2019).

3.6. Delamination method

Delamination is brought out with exclamation and sonication. Exclamation involves multiple ions or molecules (different cross-substances such as big organic blends and ions) among the scooped MXene coatings. It raises the interlayer distance among layering and increases the exterior area and apparent dissociation of films within a 2D configuration (Alhabeb et al., 2017).

To open the coatings and develop the space among the non-laminated MXene films, pretreatment before sonication intercalation is committed to absorbing ions or organic blends (Maleski et al., 2017; Li et al., 2019). Following HF etching, the OH and F operating groups form the resultant multilayer MXene exterior and evolve region. Another side, the net selectivity of mark contaminants improves after embolism owing to replacing other cations from interplants in the position of some preliminary functional clusters (Lukatskaya Maria et al., 2013).

Sonication is a substitutional set utilised if a straightforward concentration or volume of the resultant MXene fragment is chosen, where the divided MXene is sonication to assemble the needed volume of fragment or 2D MXene absorption (Liu et al., 2018; Malaki et al., 2019). The production of MXene finishes via sonication that permits the control of the fragments' dimensions and the concentration of MXene. It may be accomplished through centrifugation that divides the massive MXene particles by a solution containing shorter colloidal MXene. However, centrifugation in the absence of sonication stays a restricted preference, while, in the presence of the sonication method, the concentration of MXene colloid may be grown within solution via exfoliating undissociated atoms (VahidMohammadi et al., 2019; Berkani et al., 2022).

In the meantime, numerous hurdles must be evaluated, like raising the MXenes materials via examining synthesizing MXenes from other possible MAX coatings. Substituting HF with green or slightly poisonous chemicals as the synthesis of MXenes utilizing HF is related to severe healthiness and environmental concerns and optimizing the manufacturing method to acquire MXenes in more significant amounts. Some recent investigators have been brought out to receive acceptable consequences in this regard.

4. Properties of MXene-based nanomaterials

MXenes have a novel hybrid of characteristics, such as the great electrical performance and mechanical charcterisitcs of TMCs/nitrides; functionalized shells which assemble MXenes hydrophilic and prepared to interaction with different classes; allowing steady colloidal solutions within water; and effective captivation of electromagnetic waves, that has guided to a huge numeral of implementations. Additionaly, **Table 2** exhibit the different properties of MBNs.

Table 2. shows the different properties of MXene-based nanomaterials.

Sr. No.	MXene-based nanomaterials	Properties	Ref.
1	$Ti_{n+1}C_n$ n= 1, 2, and 3	• Considerably enhanced mechanical properties by enlarging critical strains and lessens the Young's modulus	(Guo et al., 2015)
2	Ti_2CT_2 and $Ti_3C_2T_2$ (T=F, O and OH)	• Lattice constant of Ti_2CT_2 shrinks while in case of $Ti_3C_2T_2$ it expands as a result of surface termination • High transmittance • Electronic conductors and semiconductors	(Bai et al., 2016)
3	Ti_3C_2 QDs/Cu_2O Nano-wires/Cu 0-D	• Shows 8.25 times more methanol production as compared to Cu_2O Nano-wires/Cu • Significantly improved photocatalytic performance • Higher light adsorption, charge transfer and charge recombination	(Zeng et al., 2019)
4	$Ti_3C_2T_X$/ polyvinyl alcohol (PVA)	• 34% improvement in tensile strength • Nearly 80% improvement in capacitance when PVA combined with KOH	(Ling et al., 2014)
5	MXene-Carbon nano-tubes (CNTs)	• Gradual decrease in swelling from 0.09nm to 0.03nm to 0.02nm at 180°C • Show attractive anti-swelling property and remains stable for 50 h	(Sun et al., 2021)
6	Dopamine-functionalized graphene oxide (DGO)/ MXene ($Ti_3C_2T_X$)	• Exhibit water flux of (63.5 Lm^{-2} h^{-1}) 98.1% and 96.1% dye rejection ratios for direct red 28 and direct black 38 respectively	(Zeng et al., 2021)
7	MXene/Al_2O_3	• Excellent water permeability (88.8 LMH/bar) • Greater than 99.5% rejection ratio for rhodamine B and methyl blue	(Long et al., 2021)

8	Partially reduced graphine oxide/$Ti_3C_2T_X$	• Outstanding absorption capacity for organic solvents as well as for water-based corrosives • Exhibits flame retardance property up to 1300℃	(Shi et al., 2022)

4.1. Electrical properties of MXene-based nanomaterials

Typical natural MXenes are metallic and, therefore, are similar to MAX conditions. With close functional clusters across their exteriors, some MXenes may take semiconducting characteristics. Their band gaps equal the solar band by allowing bandgap arrangement into heterostructures toward optoelectronics. Following this, various semiconducting MXenes with fit bandgaps will be presented.

MXenes cover different electronic characteristics owing to their wide compositional variety, different surface functionalization probabilities, and adjustable width controllability (Khazaei et al., 2015; Liu et al., 2016a). Amidst them, entire the bare MXenes and the bulk of surface-functionalized MXenes are metallic. This is understood that the work functions (WFs) of MXenes are sensible to their exterior interaction: for a relaxed MXene, associated with the bare exterior, the OH (O) design continuously reduces (raises) it is WF, where the F design represents either tendency depend on the specific substance. The OH-ended MXenes exhibit ultralow WFs (<2.8 eV), lower than Sc, which is approximately the lowest with elemental metals. In contrast, the WFs of a few O-ended MXenes are even more significant than Pt, with the highest WF of all elements. The WFs of F-ended MXenes constantly fall among those of OH- and O-terminated equivalents. The development of WF after exterior functionalization arises from the transformation of surface dipole moment caused by functionalization. The OH (O) end constantly points to

exterior dipole moment and therefore reduces (raises) WF, while F can include each a negative or positive exterior dipole moment reliant upon the specific MBN. Though, it is remarked that in current investigations, the blend of F, O, and OH groups at the MXene surfaces typically draws the WFs of MXenes back in an intermediary rate. Such as, with operating Kelvin probe force microscopy investigation, Xu and coworkers (Xu et al., 2016) define the WF of $Ti_2C(OH)_xF_y$, which is expected to be ≈4.98 eV. Hence, for obtaining the ultralow WF of OH (or O)-ended MXenes, subtle command of the varieties of the exterior functional clusters is essential.

4.2. Mechanical properties of MXene-based nanomaterials

MXenes' mechanical characteristics greatly depend upon their surface ends. It is divined that the O ended MXenes have very excellent toughness. Still, MXenes completed with different clusters (F and OH) exhibit lower elastic toughness than their O-ended equivalents (Bai et al., 2016). It can be compared to the distinct lattice coefficients of MXenes, including several terminations: typically, the O-ended MXenes have more miniature lattice limits than the F or OH eliminated MXenes (Zha et al., 2015). Associated with simple MXenes, the exterior-functionalized MXenes have more considerable versatility. Employing Ti_2C as a standard, Guo *et al.* (Guo et al., 2015) observe that the functionalization would overcome Young's modulus of Ti_2C, nonetheless, the functionalized Ti_2C may endure a more considerable strain than simple Ti_2C and graphene as well. The surface eliminated groups function as a buffer film for Ti_2C below tensile distortion, quieting down the destruction of Ti films and improving the rate of significant strain where Ti_2C breakages.

Computational techniques were utilized to investigate the mechanical characteristics of MXenes as per the width, surface functionalization, and compound structure. The Young's moduli of the natural MXenes were planned from the inclinations of the strain-stress graphs. Sequentially, the standards were 597, 502, and 534 GPa for Ti_2C, Ti_3C_2, and Ti_4C_3, exhibiting that the minor Ti_2C 2D single-layer film holds the most eminent Young's modulus. The higher ductile stress and bond wreckage within Ti_2C and Ti_3C_2 began near the exterior surface of the films on the point, including the maximum local stress and created to the midpoint of the carbon films. Though, for Ti_4C_3, wreckage mounted within the filmfilm's midpoint and developed until a complete break commenced to trim particle configuration (Ling et al., 2014; Borysiuk et al., 2015).

MXene/PVA catalyst films exhibit high elasticity and support 5000 folds of their load (**Fig. 7**). The micrographs of MXene-layered constructions and the mixture of MXene nanofilms along with polymers are shown in **Fig. 7**. A 40% MXene weight proportion may give Young's modulus surpassing that recognized toward PVA polymers (Pang et al., 2019).

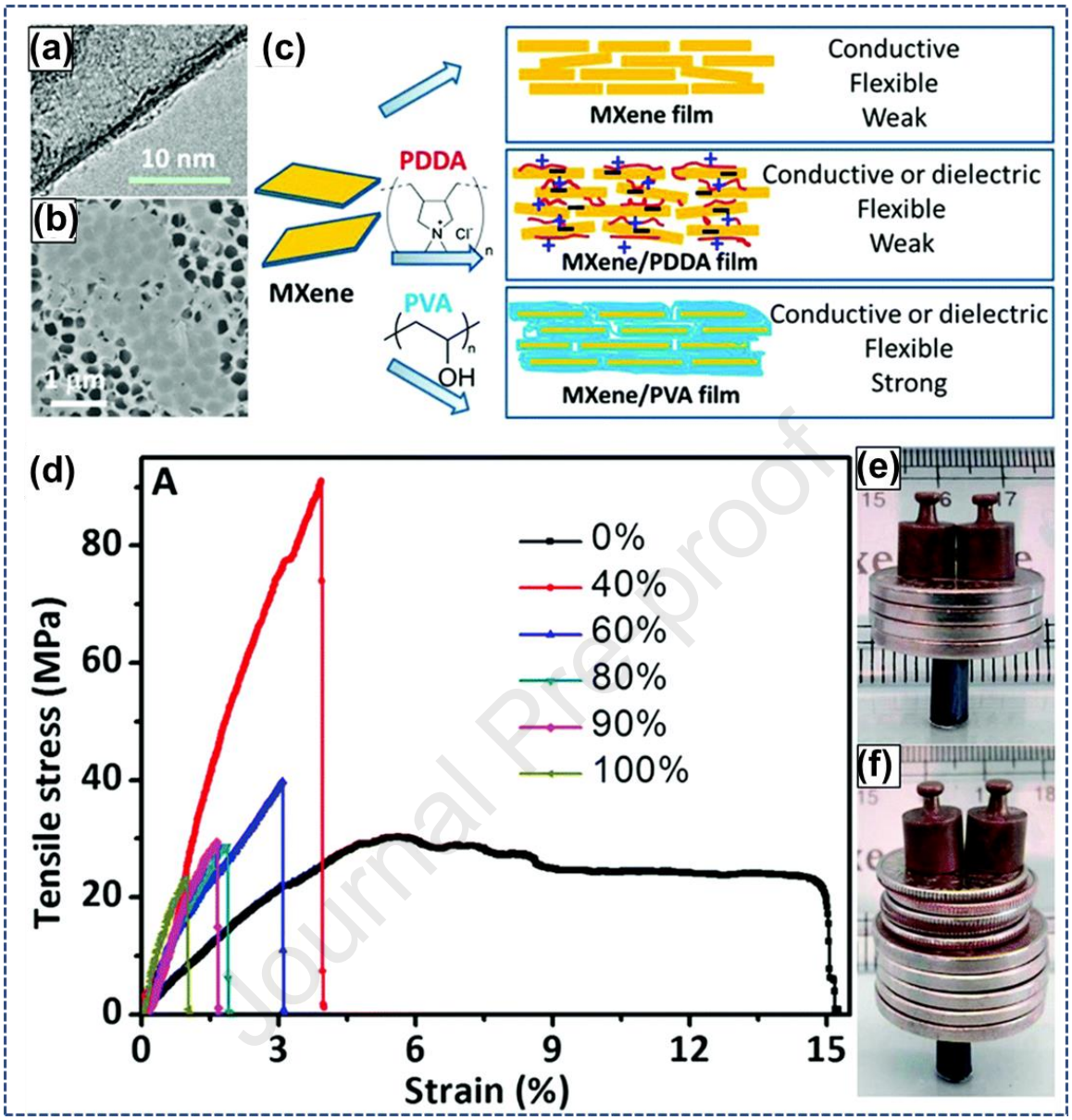

Fig. 7. MXene polymer catalyst and its mechanical characteristics. **(a and b)** Transmission electron microscopy (TEM) and SEM images of prepared MXene fragments. **(c)** Synthetic methods towards MXene sheets and MXene/polymer compound sheets. **(d)** Stress-strain graph of $Ti_3C_2T_x$/PVA composite sheets contingent upon the $Ti_3C_2T_x$ mass proportion. **(e)** Picture of a new MXene film holding 4000 folds its mass. **(f)** Images of a 90 wt% MXene/PVA composite sheet carrying 15 000 folds its mass. Reprinted with permission from Ref. (Pang et al., 2019).

4.3. Morphological properties of MXene-based nanomaterials

The crystal composition of MXenes via selective etching typically receives their MAX parents' hexagonal atomic lattice $P6_3/mmc$. The M atoms are hexagonally crammed wherever the X atoms pack the octahedral interstitial positions (Jiang et al., 2020). The lattice parameter of surface-functionalized Ti_3C_2 improvements the following inclusion and desquamate. Nonetheless, their performance was distributed MXenes sheets of 20-50 nm stiffness and length 44-90 µm. In addition, after ultrasonication into Dimethyl sulfoxide (DMSO), these MXenes were dispersed within DI water to form an aqueous media including colloidal characteristic, later refined to remove MXene (Mashtalir et al., 2013).

Additionally, Ti_3C_2 Quantum Dots (QDs)/ Cu_2O NWs catalysts were developed. Incorporation through Ti_3C_2 QDs does not transform the entire surface structure of Cu_2O NWs but resists the spongy exteriors. As exhibited with SEM, Cu_2O NWs have a spongy covering and a width of ≈500 nm (**Fig. 8 a, b**). As the processing with poly (sodium 4-styrene sulfonate) (PSS) to produce a anion charged surface upon Cu_2O NWs, Ti_3C_2 QDs grafted with cation energized Polyethyleneimine (PEI) are electrostatically self-decorated on Cu_2O NWs building hierarchical Ti_3C_2 QDs/Cu_2O NWs/Cu heterostructure. PSS and PEI particles are entirely obliterated in the argon environment through the succeeding calcination method, transmitting Ti_3C_2 QDs and Cu_2O NWs within the close connection. Covering with Ti_3C_2 QD does not change the whole surface structure of Cu_2O NWs but includes their spongy exteriors (**Fig. 8c,d**). (Zeng et al., 2019).

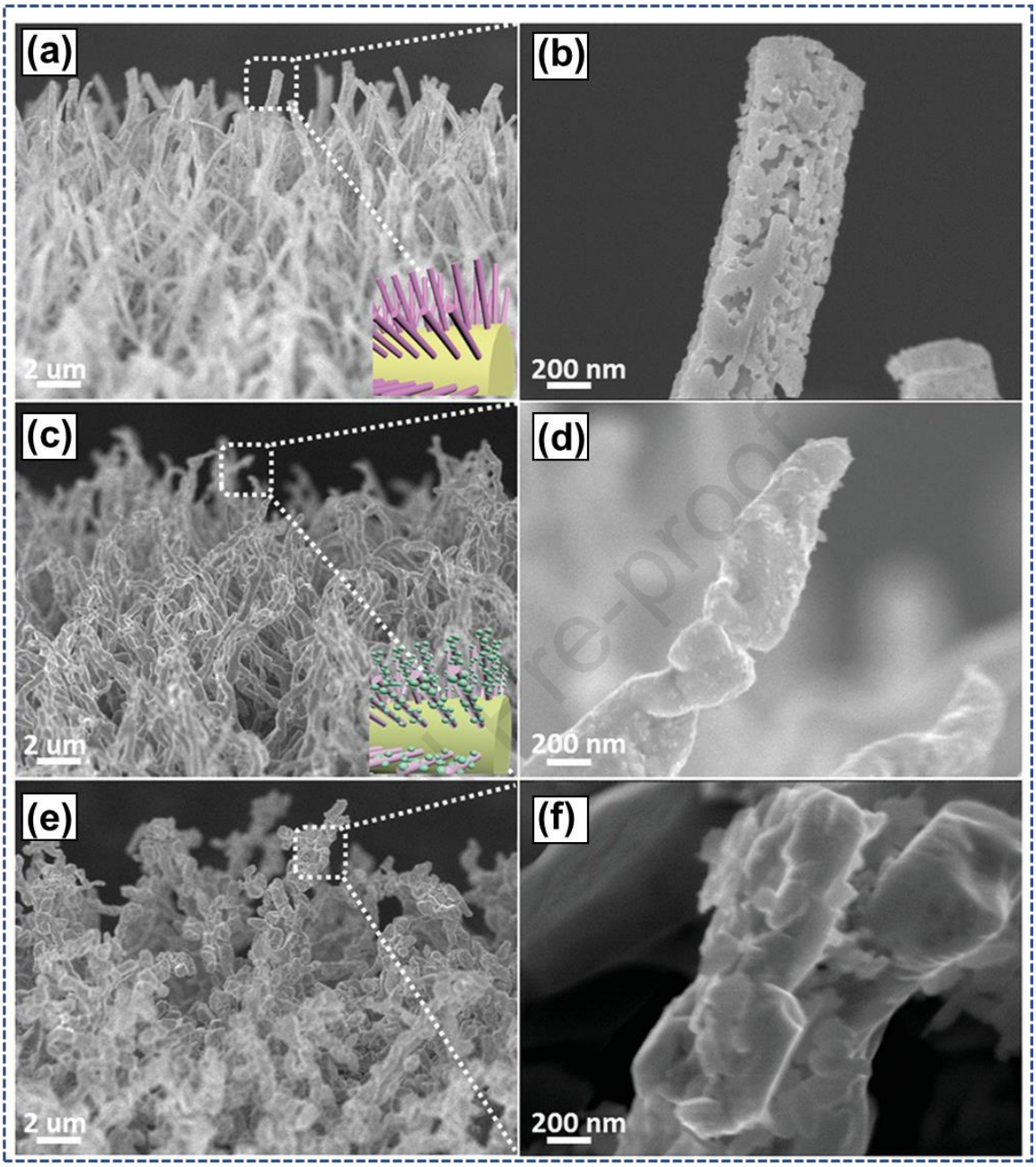

Fig. 8. Field emission SEM pictures of **(a, b)** Cu_2O NWs/Cu, **(c, d)** Ti_3C_2 QDs/Cu_2O NWs/Cu, and **(e, f)** Ti_3C_2 layers/Cu_2O NWs/Cu hetero-assemblies. Reprinted with permission from Ref. (Zeng et al., 2019).

Additionally, by examining the absorption of the MXene solutions, a slanted towards lamellar sheet construction with distinct lamellae layout from 150 to 20 μm has been achieved. While an attachment composition of hollow covered (**Fig. 9a, d**) to interlayer

coupling (**Fig. 9b, e**) or links (**Fig. 9c, f**) straight up sustained parallel sheet structure was built. The lightweight aerogel shows outstanding EMI shielding activity and a tunable proportion of electromagnetic heat observation to reflection. An ultrahigh explicit SE of 8818.2 dB cm3 g^{-1}, rising as the ultralow concentration (0.0055 g cm^{-3}) and higher EMI SE (48.5 dB) of miniature sheets, was obtained, which conferred the finest value between the described EMI shielding substances on the same time. The EMI shielding tool toward the 3D MXene aerogels may be assumed as (**Fig. 9g**):

1. a more substantial resistance match given with the 3D spongy arrangement led to more effective absorption to the occurrence of electromagnetic waves,
2. the abundance of cellular systems found within the novel 3D assembly of horizontally-situated MXene lamellae and perpendicular scaffolds improved the various observations and smattering of the occurrence of electromagnetic heat inside the bulk substance,
3. the time-changing electromagnetic currents produced in the long-array arranged MXene lamellae structure produces conductive damage and transform in temperature,
4. MXene fragments with various surface finishes and innate deficiencies occurred within the electromagnetic wave emission depending upon the dipole polarization, then recreated into a changing electromagnetic field.

3D MXene foam gathers MXene films by a vacuum filter method developed through a hydrazine-induced system (**Fig. 9h-o**). The 3D MXene foam, with self-decorated,

hydrophobic, lightweight, and supple, exhibited outstanding better electrical performance and EMI shielding activity (Lu et al., 2021b).

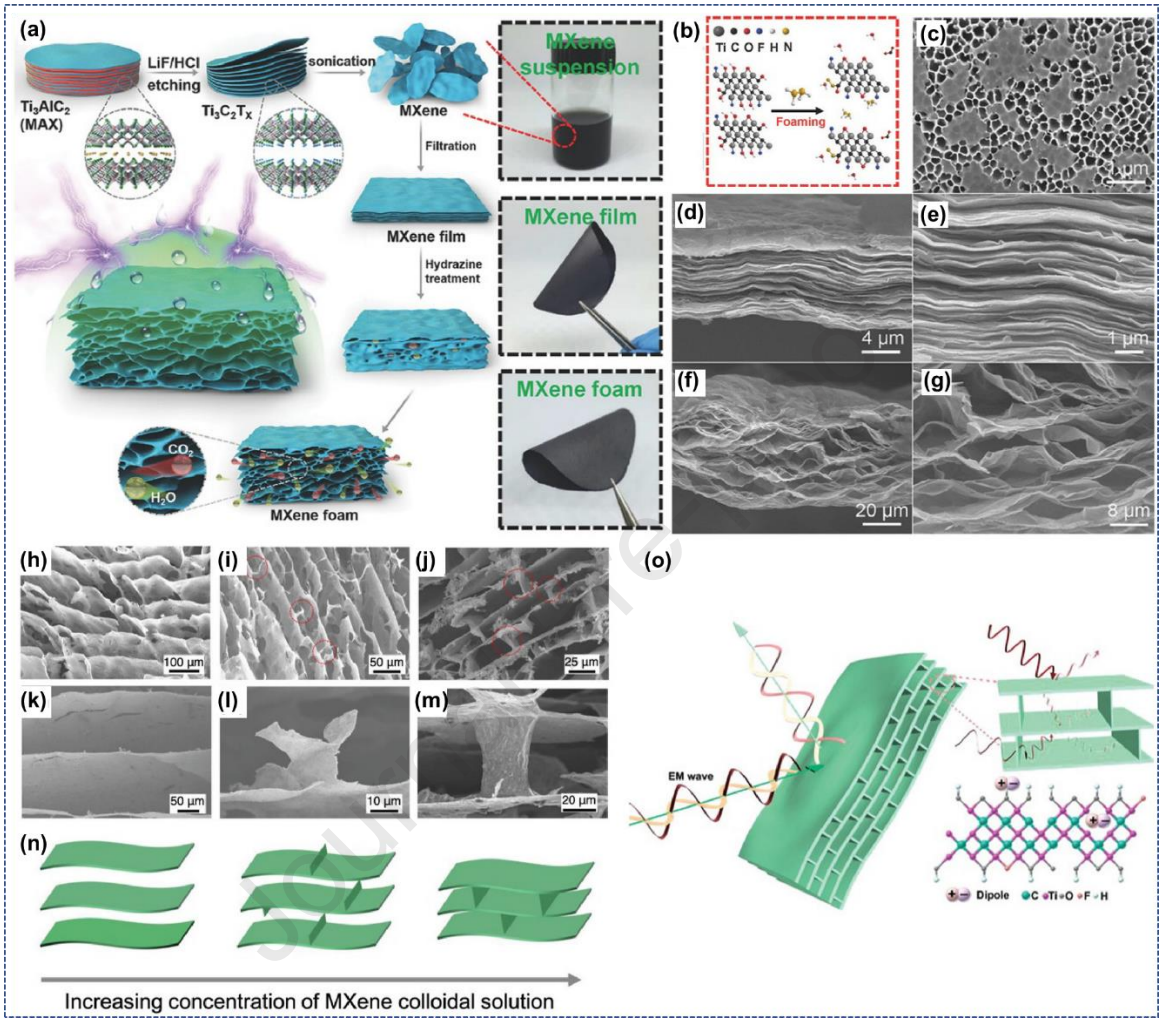

Fig. 9. (a) Graphic of the formation method of 3D MXene foam. **(b)** Hydrazine-tempted foaming device. **(c)** SEM photograph of the $Ti_3C_2T_x$ MXene films ere construction. Cross-sectioned SEM pictures of **(d, e)** the MXene sheet, **(f, g)** the 3D MXene foam. **(h-m)** SEM pictures of 3D cross-allied MXene aerogels, including distinct concentrations. **(n)** Representation of three types of compositions with enhanced MXene absorption. **(o)** The device outline toward the 3D MXene EMI shielding substance. Reprinted with permission from Ref. (Lu et al., 2021b).

5. Applications of MXene-based nanomaterials for hazardous pollutants degradation

Regarding the utilization activity of MXenes on the steady growth to development, here, we explain the broad-spectrum suitability of different MBNs within the ecological remedy. Concise information associated with environmental contaminants, structural characteristics, chemical capabilities, and construction way of MXenes is described toward the source. Later, the adsorption and deterioration sturdiness of MBNs for different pollutants, such as organic colourants, poisonous heavy metals, pesticide deposits, antibiotics, and many more, are entirely examined to determine their ability within the field of sewer water redemption and remedy (Mazari et al., 2021). **Fig. 10.** Different applications of MBNs for hazardous pollutants degradation. Also, **Table 3** shows the applications of MBNs in different pollutant degration.

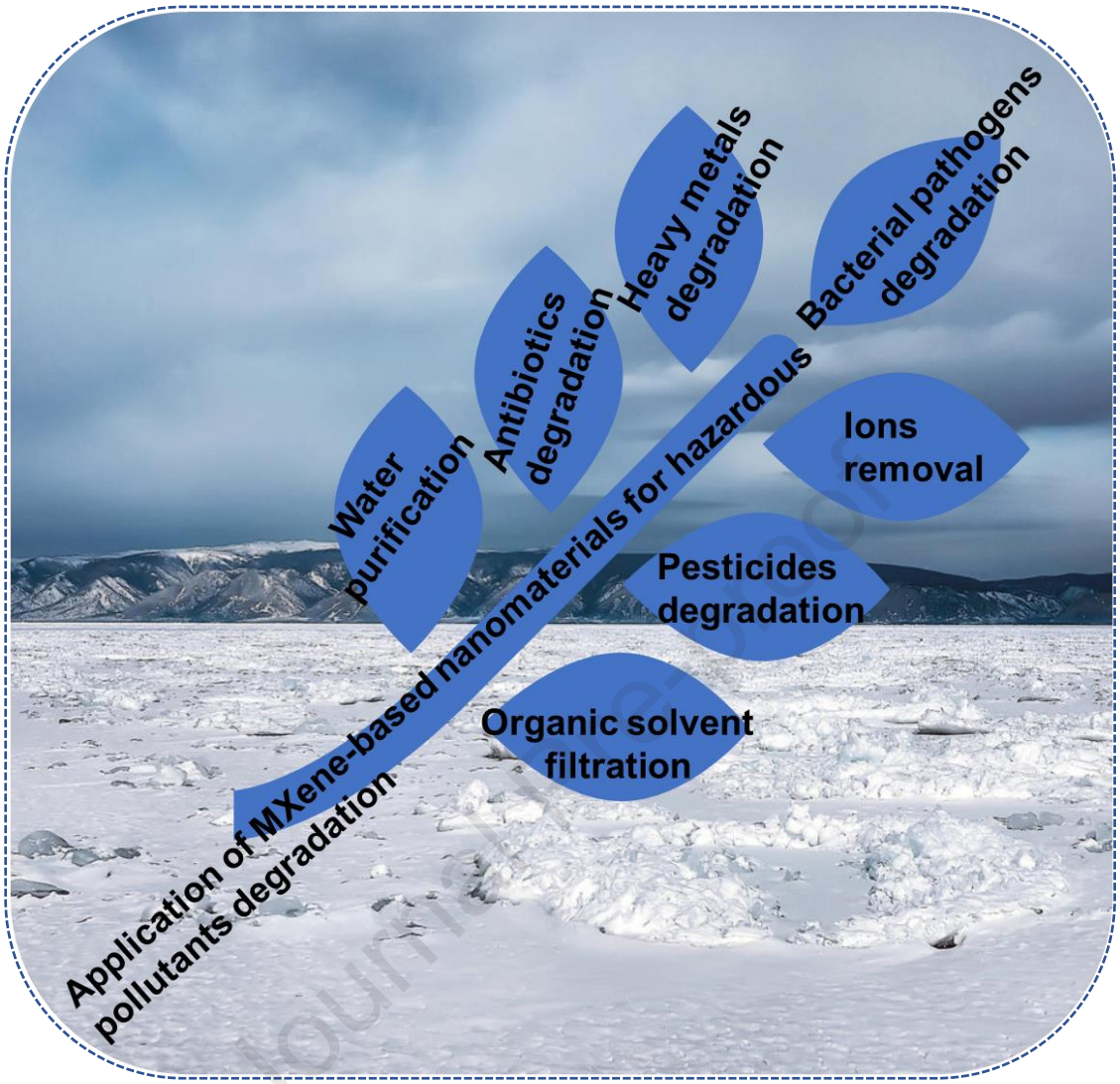

Fig. 10. Different applications of MBNs for hazardous pollutants degradation.

Table 3. The applications of MBNs in different pollutant degration.

Sr. No.	MBNs	Uses	Performance	Uptake capacity (mg/g)	Efficiency (%)	Ref.
1	$Ti_3C_2T_X$	Heavy metal (Pb(II)) removal	High adsorption capacity than graphene	36.6	-	(Jun et al., 2020a)
2	$Ti_3C_2T_X$	Removal of Ba(II), Sr(II)	Adsorb metals by ion-exchange and inner sphere complex formation	180,225	-	(Jun et al., 2020b)
3	Graphene oxide-$Ti_3C_2T_X$	Organic and inorganic pollutant removal(NaCl, Na_2SO_4, RhB, CV, MB, NR	Shows nearly 7.5 and 2.5 high water permeance as compared to pure graphine-oxide and GO/TiO_2 respectively	-	NaCl= 23 Na_2SO_4=61 RhB=98 CV=97.5 MB=99 NR=98.9	(Han and Wu, 2019)

4	Magnetic-$Ti_3C_2T_X$	Photocatalytic degradation of Diclofenac	superior stability for seven successive cycles	-	100 within 30 minutes	(Jang et al., 2020)
5	Ti_3C_2/gC_3N_4	Photocatalytic degradation of phenol	32.1% phenol was degraded under dark conditions	-	98 within 180 minutes	(Liu et al., 2020)
6	$Ti_3C_2T_X$	Organic dye (MB) removal	Excellent adsorption for cationic dyes	39	-	(Mashtalir et al., 2014)
7	$Ti_3C_2(OH)_2$	Removal of radionuclide U(VI)	Chemical adsorption and formation of hydrogen bonds was the driving force	595.3	-	(Zhang et al., 2016)
8	Ti_3C_2-Co_3O_4	Removal of Organic dye (MB)	Enhanced adsorption performance	MB=136.24 RhB=47.687	-	(Luo et al., 2019)

9	$Ti_3C_2T_X$ Ti_3CT_X $Mo_2TiC_2T_x$	Removal of Urea	No cyto-toxicity, hydrogen bond formation with functional group	21.7 6.6 8.4	-	(Meng et al., 2018)
10	$CuFe_2O_4/Ti_3C_2$	Photocatalytic degradation of Sulfamethazine (SMZ)	Enhanced synergistic degradation under visible light	-	59.4	(Cao et al., 2020)
11	CeO2/Ti3C2-Mxene	Photocatalytic degradation of tetracycline	6.3 times better performance than bare CeO2	-	80.2	(Shen et al., 2019)
12	$Ti_3C_2T_X$ core-shell spheres with alginate	Removal of Hg(II) ions	Exhibit unique structure and act as excellent adsorbent	932.84	100	(Shahzad et al., 2019)

13	Ag-$Ti_3C_2T_X$	Removal of RhB MG	Exhibit excellent water flux	-	RhB=82% MG=94.6%	(Pandey et al., 2018b)
14	g-C_3N_4/Ti_3C_2	Removal of ciprofloxacin	Schottky junction inhibit the electron hole	-	100 within 2 hours	(Liu et al., 2019a)
15	TiO_2-$Ti_3C_2T_X$	Elimination of dextran	Short the manufacturing process and reduce membrane cost	-	Molecular weight >30kDa= >95	(Xu et al., 2018)

5.1. Water purification by MXene-based nanomaterials

Recently, the growth of new NMs toward water processing has drawn more and more attention (Ahmed et al., 2021)(Patial et al., 2021). MXenes is a universal name for various 2D TMCs and carbonitrides substances with graphene-like constructions (Abbasi et al., 2021). As a novel 2D lamellar nanomaterial, numerous investigations have concentrated on designing and synthesizing MBNs due to their sizeable inter-layer annulled by the 2D stacking composition and a sizeable definite surface area rich adaptable surface working group, and durable hydrophilicity. Regarding their different characteristics, the associated analysis and potential of 2D MBNs toward layer detachment and water processing utilization are presented. Sequentially, a GO-MXene-TiO_2 film showed around 7.5- and 2.5-times more excellent water penetrability (90 L/m^2 h bar) than a pure GO film and a GO-TiO_2 layer. Successively scattered laminar-arrangement TiO_2 nanocrystals were utilized as inlay that provided consistent nanochannels in the GO film for H_2O particle carrier, while MXene storing also contributed more nanochannels to the water carrier. High extraction speeds of different colourants (for example, Rhodamine B (RhB) and methyl blue (MB)) were completed by the GO-MXene-TiO_2 film; though, the elimination speeds of inorganic salts were comparatively low. Extraction of the colourants with adsorption was very quiet (around <10%), indicating that different tools, for example, size separation and/or electrostatic synergy were imperative during the transport of organic colourants. By the way, a graphic of the fib of **Fig. 11(a)** the synthesized membranes were expressed as HGMX membrane, while *X* is the mass proportion of MXene **Fig. 11(b)** GO/TiO_2 membrane developed *through* a conventional approach. Pure water penetrability and denunciation of RhB of **Fig. 11(c)** HGMX film and **Fig. 11(d)** GO/TiO_2 film. **Fig. 11(e)**

Water penetrability of HGM30 toward separate colourants, **Fig. 11(f)** common rejection and adsorption rejection through the HGM30 film toward organic colourants (Han and Wu, 2019).

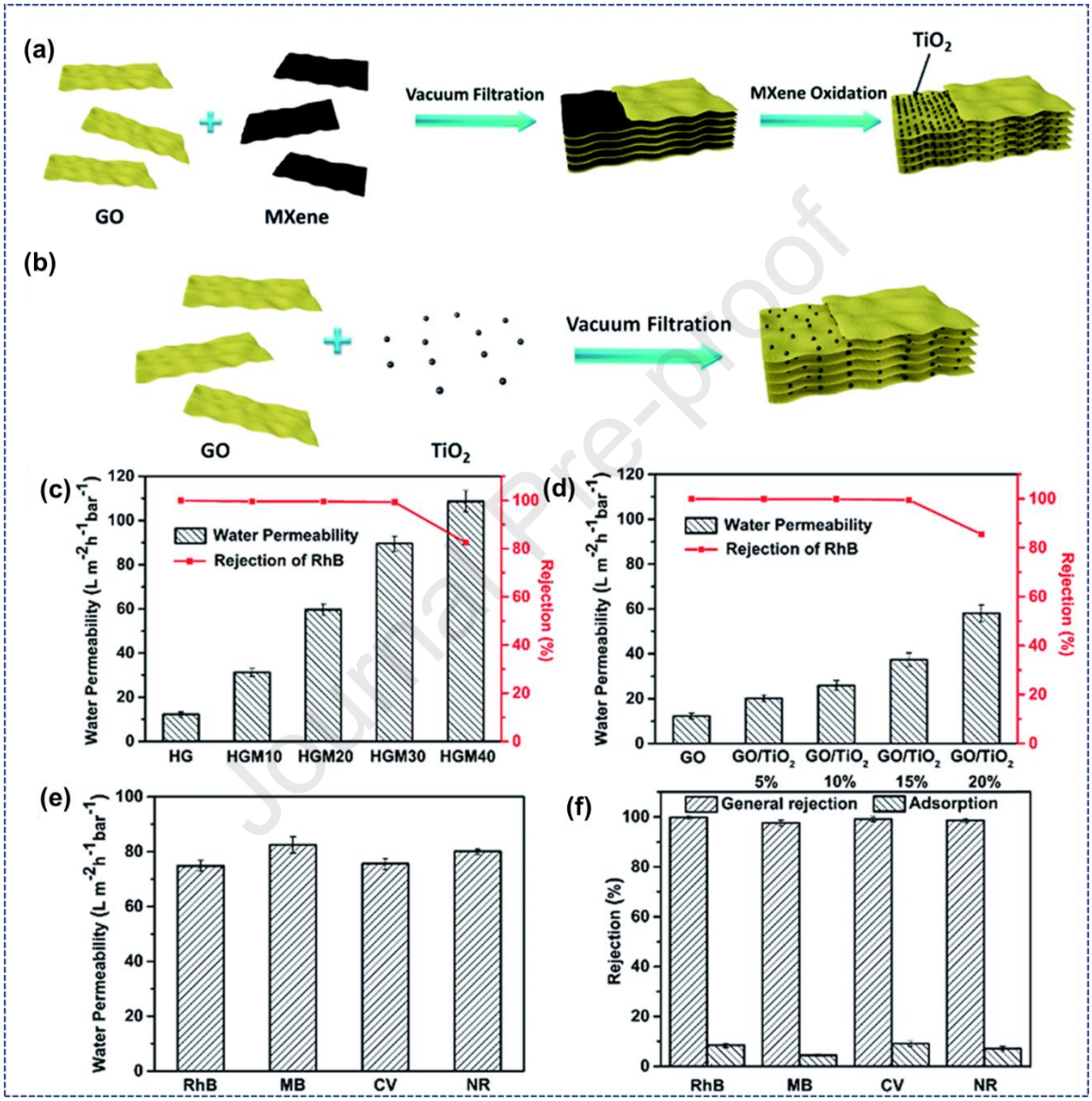

Fig. 11. Graphic of the assembly of **(a)** HGMX film, **(b)** GO/TiO_2 film arranged *through* a conventional technique. Clean water penetrability and refusal of RhB of **(c)** HGMX film and **(d)** GO/TiO_2 membrane. **(e)** Water penetrability of HGM30 towards distinct colorants, **(f)** overall refusal and adsorption refusal through the HGM30 film towards organic colorants. Reprinted with permission from Ref. (Han and Wu, 2019).

5.2. Organic solvent filtration by MXene-based nanomaterials

The practice of MXenes has also been recognized within the catalytic elimination/degeneration of ecological contaminants in the absence of radiation. In this regard, the catalytic operation is organized to enhance the oxidants complete activity or reductant to obtain the entire degeneration or mineralization of the contaminants. **Table 4** compiles the MBNs published toward the photodegradation of the ecological contaminants.

Table 4 Shows the photodegradation activity toward the organic dyes by utilizing Mxene-based materials photocatalysts.

Sr. No.	**Mxene-based nanomaterials**	**Dyes**	**Absorption (mg L^{-1}) and volume (mL)**	**Degradation efficiency with time**	**Ref.**
1	$Ti_3C_2T_x$	MB	1.2×10^2 and 40	81% within 5 h	(Mashtalir et al., 2014)
2	Bi_2WO_6/Nb_2CT_x	RhB	15 and 100	99.8% within 90 min	(Cui et al., 2020)
3	TiO_2/Ti_3C_2	MO	20 and 100	98% within 30 min	(Gao et al., 2015)
4	$Ti_3C_2/TiO_2/CuO$	MO	20 and 100	99% within 80 min	(Liu et al., 2017b)
5	Ag_3PO_4/ Ti_3C_2	MO	20 and 50	-	(Cai et al., 2018)
6	TiO_2@C	MB	20 and 50	85.7% within 6 h	(Li et al., 2018a)
7	In_2S_3/TiO_2@ $Ti_3C_2T_x$	MO	20 and 100	92.1% within 1 h	(Wang et al., 2018)
8	CdS@Ti_3C_2@TiO_2	RhB	20 and 200	100% within 1 h	(Liu et al., 2019b)

9	Ag_3PO_4/ Ti_3C_2	Aniline	-	81.8% within 8 h	(Ding et al., 2019)
10	CeO_2/Ti_3C_2	RhB	20 and 50	75% within 90 min	(Zhou et al., 2017)
11	Fe_2O_3/Ti_3C_2	RhB	10 and 100	98% within 2 h	(Zhang et al., 2018a)
12	$Ti_3C_2T_x$/GO/EY	4-NA	10 and 20	97% within 5 min	(Chen et al., 2019)
13	$BiOBr_{0.5}I_{0.5}$/ $Ti_3C_2T_x$	RhB	20 and 100	100% within 40 min	(Shi et al., 2019)

MO-methyl orange, *4-NA*-4-nitroaniline

GO-MXene catalysts films have been estimated toward their possibility towards organic solvent nanofiltration purposes (Wei et al., 2019). Alike to a previous investigation (Yang et al., 2017), films that fabricated only GO exhibited very unproductive saturation toward usually utilized organic solvents, for example, acetone and low molecular weight of alcohols. Though, membranes that included only MXene revealed better permeance toward absolute organic solvents. While reasonably comparable penetration was recognized even among MB dismissal within these solvents, lower MB elimination (<2%) was perceived to the MXene-only film (Wei et al., 2019).

Based upon the overextended studies, (i) nature of the interfacial synergy among 2D Ti_3C_2 nanofilms and TiO_2 nanostructures, (ii) improved TiO_2 contented at Ti_3C_2 (below ignition and hydrothermal process), (iii) manifold heterojunction production, (iv) necessary oxygen vacancy production within the TiO_2 and (v) substitute of functional combinations exceptionally advanced the various dye degeneration, drug dissolution, CO_2 mitigation and

N_2 photo obsession. In this way, **Fig. 12** exhibits the multi-faceted TiO_2/Ti_3C_2 composite use toward photocatalytic performance (Sreedhar and Noh, 2021).

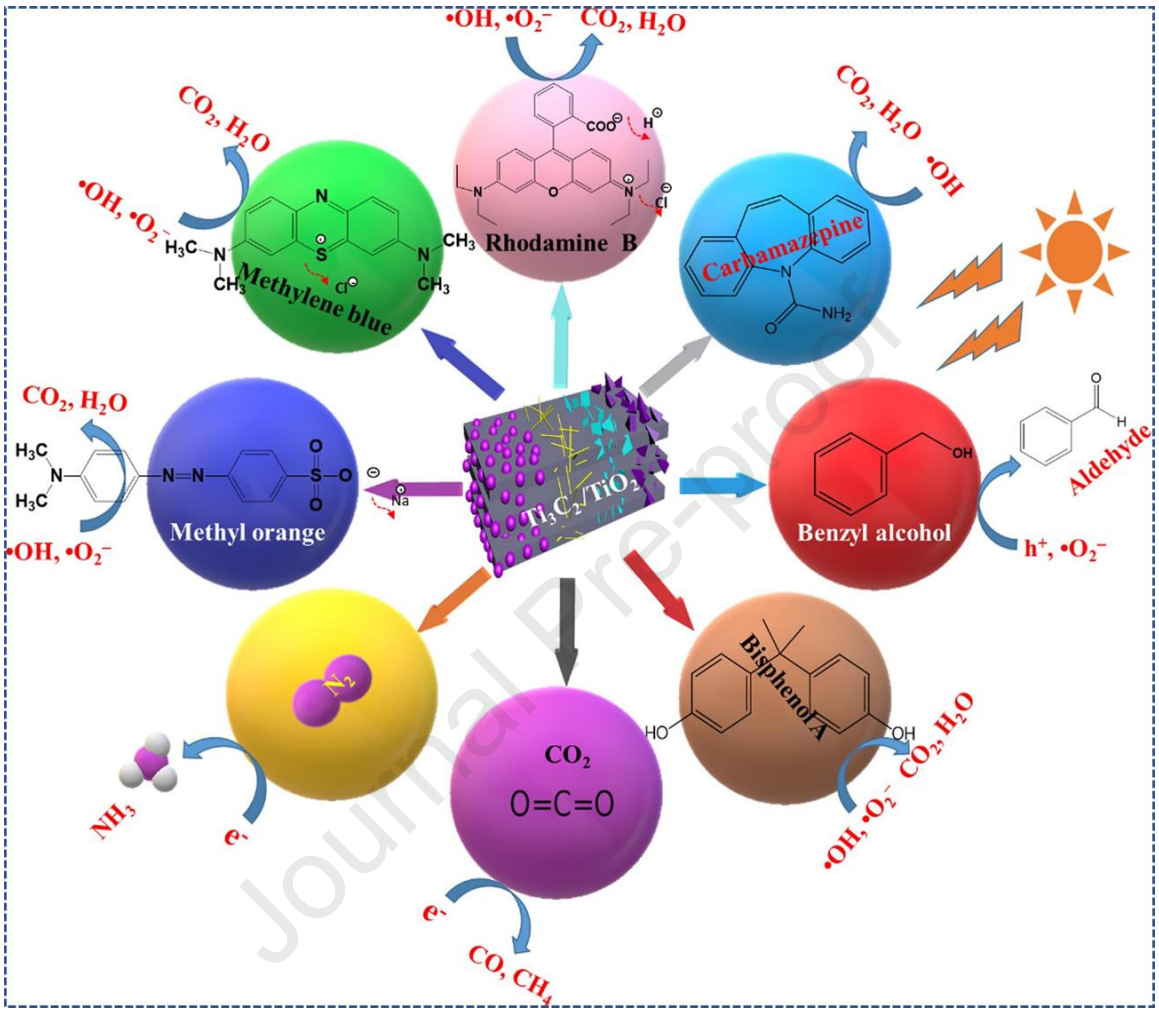

Fig. 12. Graphic design of Ti_3C_2/TiO_2 compound towards different dye deprivation activities. Reprinted with permission from Ref. (Sreedhar and Noh, 2021).

GO-MXene material films have been assessed concerning their latent towards organic solvent nanofiltration purposes. **Fig. 13(a)** GO/MXene composite lamellar films used for effective solvent penetration and molecular detachment. **Fig. 13(b)** Flux of MB organic solutions by GM-70% films as converse thickness to solvent. **Fig. 13(c)** shows the correlation graph of MB solubility into different solvents and the MB refusal rate of GM-

70% films. **Fig. 13(d)** XRD patterns of GM films moistened with different solvents. **Fig. 13(e)** Detachment appearance of GM-70% films for different dyes demise in CH_3CH_2OH and CH_3OH (Wei et al., 2019). Compared to a previous investigation (Yang et al., 2017), films combined only GO confirmed very inefficient penetration for generally applied organic solvents, for example, CH_3COCH_3, $CH_3CHOHCH_3$, CH_3CH_2OH, and CH_3OH. Though, films that included only MXene conferred better permeance toward natural organic solvents.

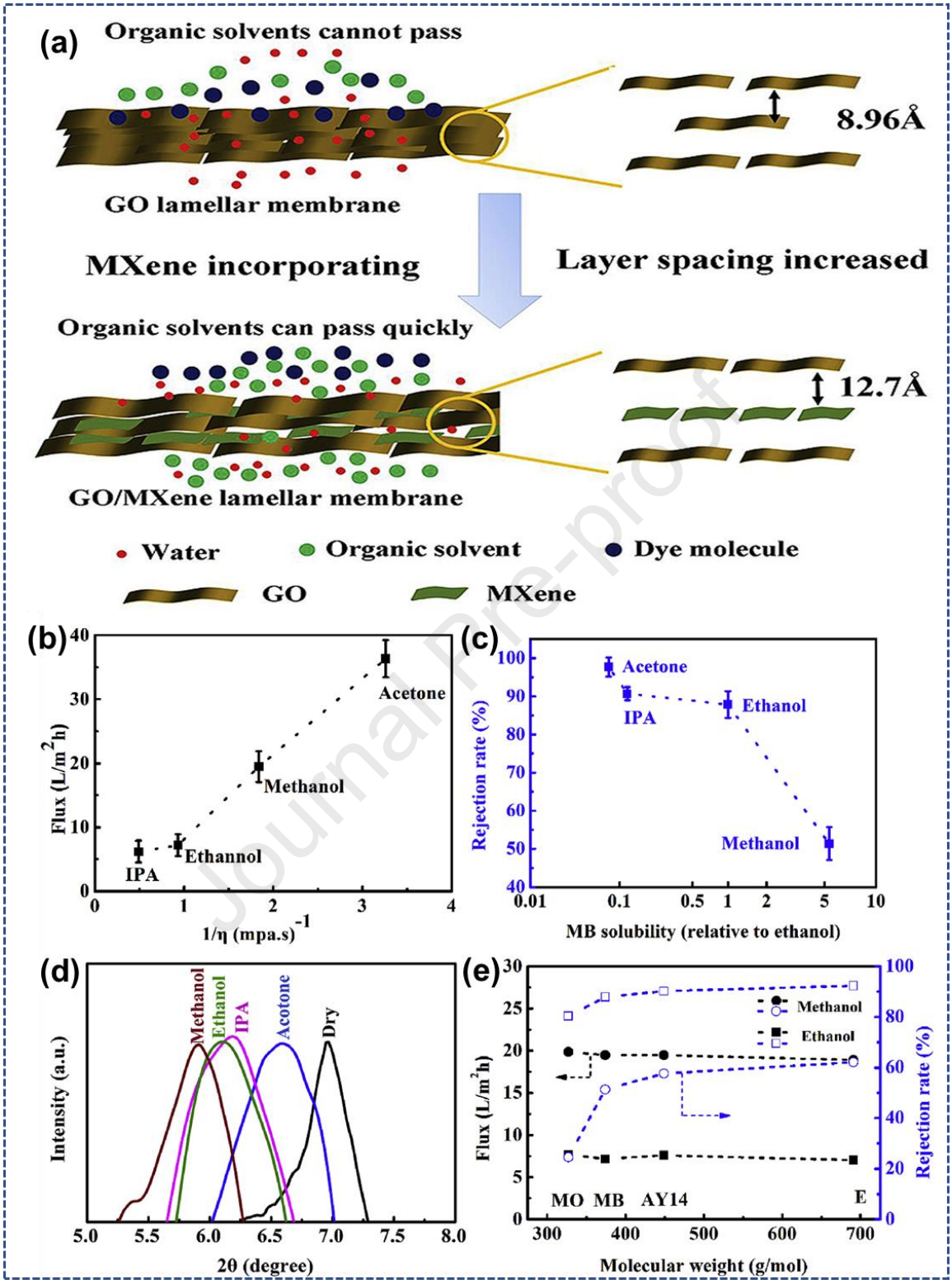

Fig. 13. (a) GO/MXene catalyst lamellar films toward effective solvent penetration and molecular detachment. **(b)** The flux of MB organic dyes by GM-70% layers as a function of reverse thickness concerning solvent. **(c)** Correlation graph of MB dissociation into different solvents and the MB

dismissal rate of GM-70% films. **(d)** XRD graphs of GM films moistened through different solvents. **(e)** Severance exhibition of GM-70% films toward different dyes extinction within CH_3CH_2OH and CH_3OH. Reprinted with permission from Ref. (Wei et al., 2019).

5.3. Antibiotics degradation by MXene-based nanomaterials

Antibiotics are infiltrating the actual circumstances global due to their widespread adoption, and this increase pretends important warnings to human well-being and environmental protection. Simultaneously, more effective strategies toward antibiotic discovery and elimination are crucially required. The extensive utilization of antibiotics has been advanced within defending humans and cattle from pathogens and encouraging the advancement of drugs, farming, aquaculture, and other areas (Rehman et al., 2015). This large-scale application of antibiotics has commenced their infiltration within the eco-friendly atmosphere (Martinez, 2009). Few antibiotics, for example, tetracycline and oxytetracycline, are incredibly determined, and their consumption within the atmosphere increases. These tenacious antibiotic deposits have a notable negative influence on human well-being and environmental protection. Therefore, the misuse of antibiotics executes it frequently essential to explore available, cost-effective, practical, and environmentally benign approaches toward their discovery and elimination (Lu et al., 2021a). The number of articles within Scopus articles with keywords, like MoS_2, hexagonal boron nitride (h-BN), layered double hydroxides (LDHs), g-C_3N_4, TMCs and nitrides (MXenes) + antibiotics + discovery, degeneration, and adsorption has grown significantly during the latest five years (**Fig. 14a-d**). As per their chemical construction, generally utilized antibiotics can be categorized as b-lactams, fluoroquinolones, macrolides, sulfonamides, tetracyclines, and aminoglycosides (**Fig. 14e**).

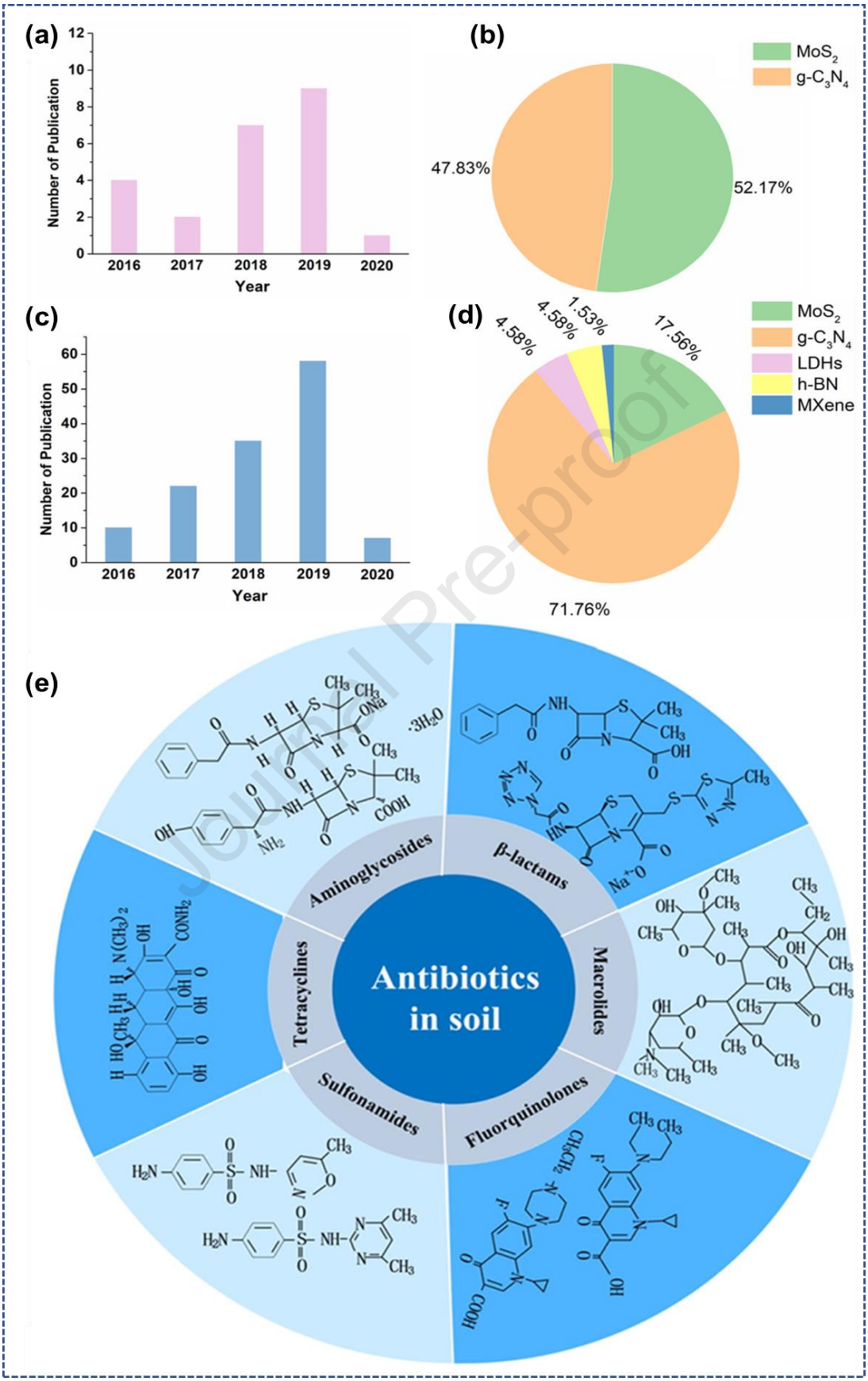

Fig. 14. **(a, c)** Numbers of papers describing 2DMs-bg-based techniques toward the discovery **(a)** and elimination **(c)** of antibiotics; **(b, d)** Percentages of various 2DMs-bg practiced within the discovery **(b)** and elimination **(d)** of antibiotics. **(e)** Distribution and chemical compositions of few typical antibiotics identified inside soil. Reprinted with permission from Ref. (Lu et al., 2021a).

To overwhelm the antibiotics issues, (Cao et al., 2020) created a novel $CuFe_2O_4$/MXene (CFO/Ti_3C_2) heterojunction material toward visible radiation supported photocatalytic degeneration of sulfamethazine. They increased the photoinduced transporters' existence by incorporating Ti_3C_2 and intervening, including the photogenerated electron holes rearrangement. Outcomes showed intense synergistic degeneration of as-incorporated photocatalyst, transferring around 60% elimination of sulfamethazine (Zhang et al., 2021).

5.4. Pesticides degradation by MXene-based nanomaterials

Pesticides are chemicals employed to prevent and eradicate pests and weeds and defend agricultural manufacture. Currently, the exogenous stimuli active controlled-release pesticide delivery system (PDS) has attracted growing recognition (Feng et al., 2021). A well-arranged exact liberation PDS can decrease the direct connection of insecticides and atmospheric conditions, overwhelming the rupture discharge mode of available pesticides. Moreover, it may also reduce the atmospheric hazard of pesticides by lessening pesticides' amount and spray regularity. Amongst several stimuli-active PDSs, pH is the commonly applied inducement. Similarly, Hao *et al.* (Hao et al., 2020) published a pH-active exact discharge operation utilizing boron nitride (BN) as the messenger. They discovered that by electrostatic synergies, π-π assembling, and the hydrophobic force, the insecticide would be efficiently placed. The liberation function of the pesticide from BN would be influenced by pH value. Lin and his coworkers received a double-layer insecticide transporter utilizing MOFs and sodium lignosulfonate (Huang et al., 2021). The prior investigations have made

several practical examinations; however, developing more facile, effective, multifunctional, and reliable carriers is yet required. Although pesticide quantification techniques have been broadly defined within the research, only a rare study have accompanied on-site pesticide residue investigations. Therefore, Umapathi *et al*. (Umapathi et al., 2021) provide a thorough summary of the colourimetric-based on-site sensing approaches for rapidly detecting pesticides within agricultural feeds.

The 2D Ti_3C_2 nanofilms were made by HF etching of MAX stage Ti_3AlC_2 and liquid-phase shedding (**Fig. 15a**). Ere HF processing, the Ti_3AlC_2 offers compact stacking sheets (**Fig. 15b**). After removing the Al sheet from Ti_3AlC_2, the construction Ti_3C_2 bulk becomes fluffy, comparable to an exposed accordion (**Fig. 15c**). Also, the avermectin (AV) content of AV@Ti_3C_2 displays no noticeable variation (**Fig. 15d**), which meets practical product and purpose requirements. To verify the photostability of AV@Ti_3C_2, the degeneration speed of AV and AV@Ti_3C_2 on different periods. Free AV is sensitive when revealed below UV light, including a degeneration flow of about 94.07% during the initial 8 h (**Fig. 15e**). At the same time, the degeneration speed of AV@Ti_3C_2 is just 19.35% subsequent 48 h radiation (**Fig. 15f**). By outfitting the investigational results by the kinetic degeneration pattern, the half-life of AV@Ti_3C_2 (176 h) is 102.3-times compared to free AV (1.72 h) (**Fig. 15g**) (Song et al., 2021b).

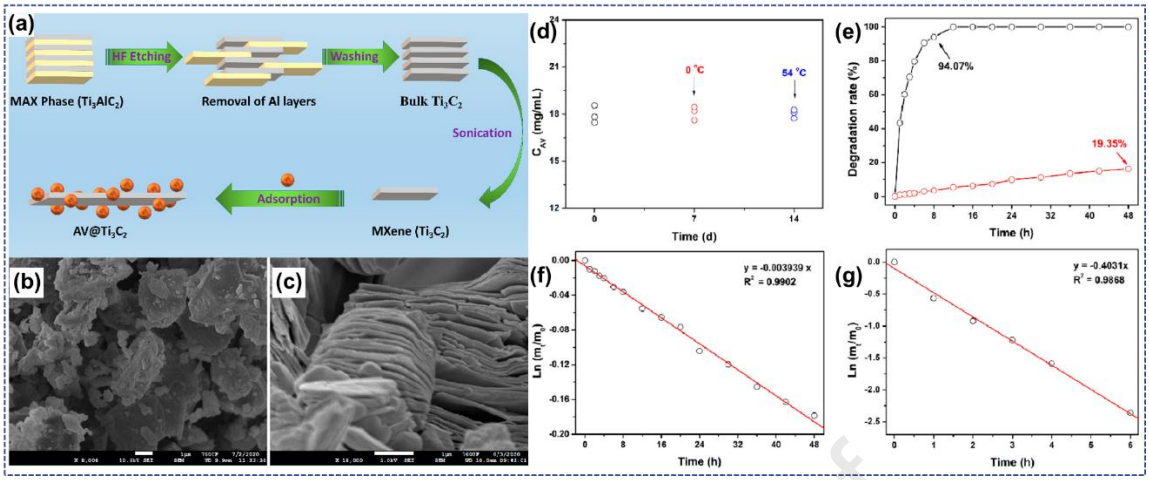

Fig. 15. **(a)** Construction of MXene facet Ti_3C_2 and its utilization for AV control and Insect controller. SEM pictures of **(b)** Ti_3AlC_2, **(c)** bulk Ti_3C_2. **(d)** AV content of AV@Ti_3C_2 after collecting on 0 °C around 7 d and 54 °C around 14 d. **(e)** The degeneration rate of AV and AV@Ti_3C_2 below UV radiation toward 48 h. **(f)** Degradation kinetics of AV@Ti_3C_2. **(g)** Degeneration kinetic of AV. Reprinted with permission from Ref. (Song et al., 2021b).

5.5. Heavy metals degradation by MXene-based nanomaterials

Effectual approaches for terminating harmful metals from wastewater have significantly reduced freshwater lack. Because of its outstanding removal efficacy, simplicity and economical at ambient circumstances, adsorption is one of the utmost capable purifying methods. MBNs have been proven to be suitable adsorbents in various toxic metal removal applications. Commonly, heavy metals ought atomic weights varied within 63.5 and 200.6 by a density superior to 5 g/cm^3 (Srivastava and Majumder, 2008). Removing several manufacturing wastewaters into water forms is one of the leading causes of heavy metal discharge within the atmosphere. Like organic contaminants, heavy ores are non-biodegradable that serve to expand within existing bodies. Industrial wastewater usually includes many heavy metals, for example, Cu, As, Ni, Hg, Zn, Pb, Cd and Cr (Ihsanullah et al., 2016).

In addition, the MXene surface-functionalized characteristics also performed an essential part in improving the adsorption performance. Titanium-based MXenes (i.e., $Ti_3C_2T_x$) nanofilms were the commonly published adsorbent concerning heavy metal ions. MXene nanocomposite also showed exceptional performance upon different heavy metal ions elimination employing the adsorption method (Fard et al., 2017). As revealed in **Fig. 16(a, b)**, the barium adsorption mode of MXene is pH-responsive. The dependence may be associated with both elements existing within the adsorbent and the chemistry of the suspension. Shahzad *et al.* (Shahzad et al., 2018) developed composite $Fe_2O_3/Ti_3C_2T_x$ catalysts and used them to eliminate Hg (II) ions. After consolidating Fe_2O_3 at the $Ti_3C_2T_x$ exterior, the particular surface area was improved by 56.5 to 68.89 m^2/g. The compounds showed a much-rectified adsorption acceptance execution of 1128.41 mg/g next 20 min of adsorption. To assess the impact of pH upon the adsorption performance of the magnetic $Ti_3C_2T_x$ MXene *(MGMX)* composite toward Hg(II) with a combination of tests was conducted within an extent of pH 2-9 on ambient condition utilizing 0.025 g L^{-1} of the nanomaterials within a 10 mg L^{-1} Hg(II) suspension inside the **fig. 16(c, d)**.

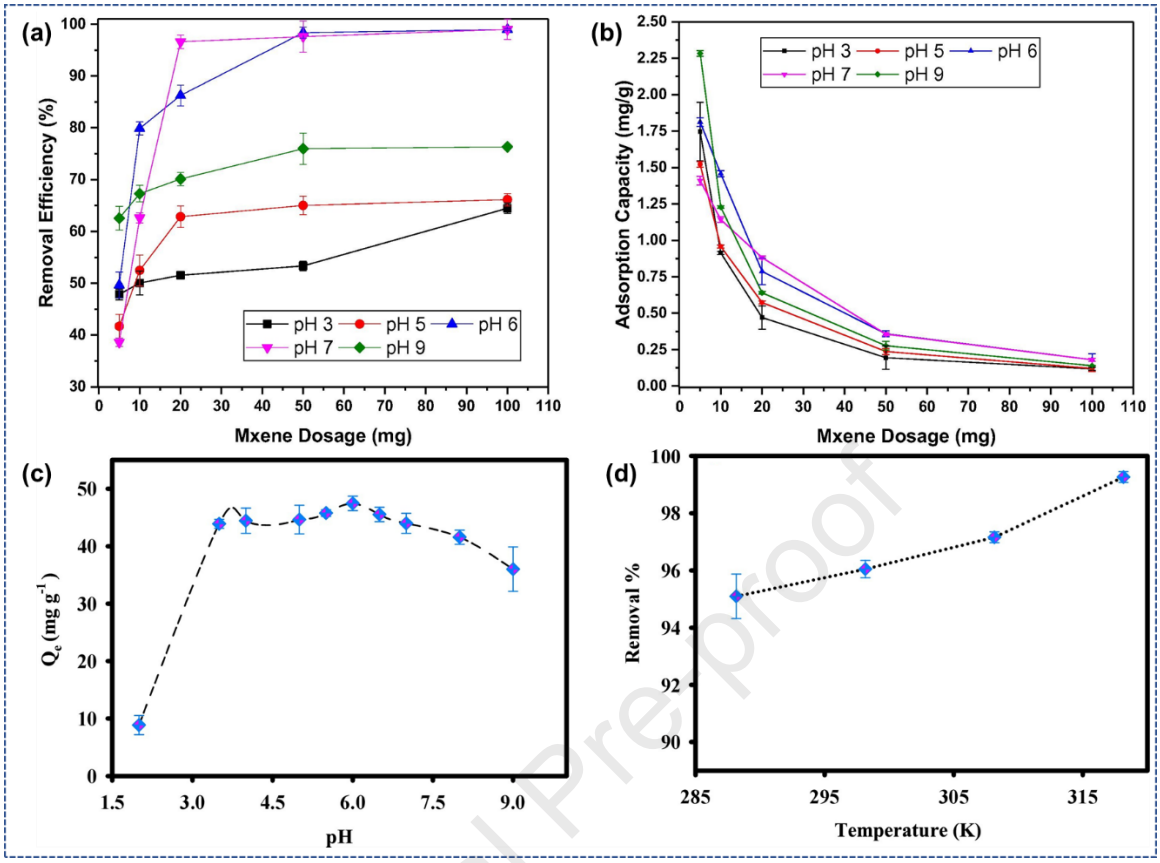

Fig. 16. Impact of pH on adsorption potential **(a)** and elimination ability **(b)** of barium employing MXene. Change within Hg(II) elimination potential caused through variations in **(c)** suspension pH and **(d)** heat. Reprinted with permission from Ref. (Shahzad et al., 2018).

Further, Zou *et al.* (Zou et al., 2016) compared the acceptance capabilities of urchin-similar rutile titania carbon (C-TiO_2) catalyst (u-RTC) and $Ti_3C_2(OH)_{0.8}F_{1.2}$ MXene opposite the elimination of Cr (VI) ions. The nanomaterials showed about 4.2 folds greater adsorption appearance compared to those of the absolute $Ti_3C_2T_x$ MXene under the appearance of different anions, for example, Cl^-, NO_3^- and SO_4^{2-}. Furthermore, the levodopa-incorporated $Ti_3C_2T_x$ MXenes also exhibited developed Cu(II) ions elimination from sewer water, and MBNs were also capable of extracting Cr(VI), Ag(I), Pd(II) and Au(III) ions by an aqueous suspension. All sheets were reconstructed, including HCl and NaOH solution and reprocessed (Xie et al., 2019; Jaffari et al., 2021).

5.6. Ions removal by MXene-based nanomaterials

Different organic contaminants, heavy element ions do not degenerate into existing organisms but grow over the period, causing more critical harm to bodies(Chandel et al., 2020; Raizada et al., 2020; Thakur and Thakur, 2015, 2014, 2014; Thakur and Voicu, 2016). Hence, it is essential to separate heavy metal ions from pure water (Cui et al., 2015; Gu et al., 2018). MXenes and their byproducts with high O_2-comprising assemblies and substantial surface areas have drawn massive recognition as suitable adsorbents toward heavy metal positive ion replacement (Fu et al., 2018; Wu et al., 2019). Significantly, investigation shows that TM ingredients included in MXenes have a great adsorption connection toward several heavy element ions (Hua et al., 2012). Newly, Peng and his coworkers (Peng et al., 2014) summarized that an alk-MXene form ($Ti_3C_2(OH/ONa)_xF_{2-x}$), including alkalization intercalation, exhibits novel adsorption performance to Pb(II). A range of group adsorption investigations showed that alk-MXenes control unique head adsorption capability (140 mg g^{-1}); ideally, the highest hypothetical adsorption potential is approximately 2800 mg g^{-1}. Furthermore, the fancied particular adsorption characteristics of Pb(II) were affirmed. The outcomes reveal that its coexistence hardly influenced the elimination ability of Pb(II) with typical contending positive ions, with Mg(ii) and Ca(II). These outcomes explained that MXenes had noted the potential for functional application into Pb(II) elimination after aqueous media. Motivated with this investigation and ongoing theoretical analysis at the adsorption machinery of Pb(ii) were summarized depending upon the research of the first-principles computations (Chen et al., 2020).

Lately, $Ti_3C_2T_x$ was initially published to overcome BrO_3^- to Br^- in an aqueous media efficiently. The lessening characteristics of MXenes for BrO_3 were estimated; **Fig. 17(a)**

explains that the decreasing ability rises with the addition into the $Ti_3C_2T_x$ absorption till it moves capable of 15 mg L^{-1} the elimination ability ultimately ends 321.8 mg g^{-1} in 50 min. As recorded within (**Fig. 17b**), up to ~37.5 μmol/L of bromate were decreased near ~100%. Following this density, the performance started to decline and attained a 45% decline on 67.5 μmol/L. As recorded under **Fig. 17(c)**, ~100% conversion of BrO_3^- was seen without coexisting ions, while nearly 92% loss of BrO_3^- was obtained; this slight reduction was observed slightly decreased shows a minimum influence opposing ion. It exhibited the remarkable selectivity of MXene approaching BrO_3^- decrease. **Fig. 17(d)** shows the XRD pattern before and after conversion; TiO_2 and amorphous carbon formation were affirmed during the reduction method, indicating that the decrease presents an advanced performance after the adsorption upon the exterior $Ti_3C_2T_x$. **Fig. 17(e, f)** confers the SEM micrographs, describing the lamellar MXene's morphology before and after converting BrO_3^- within an aqueous solution (Pandey et al., 2018a).

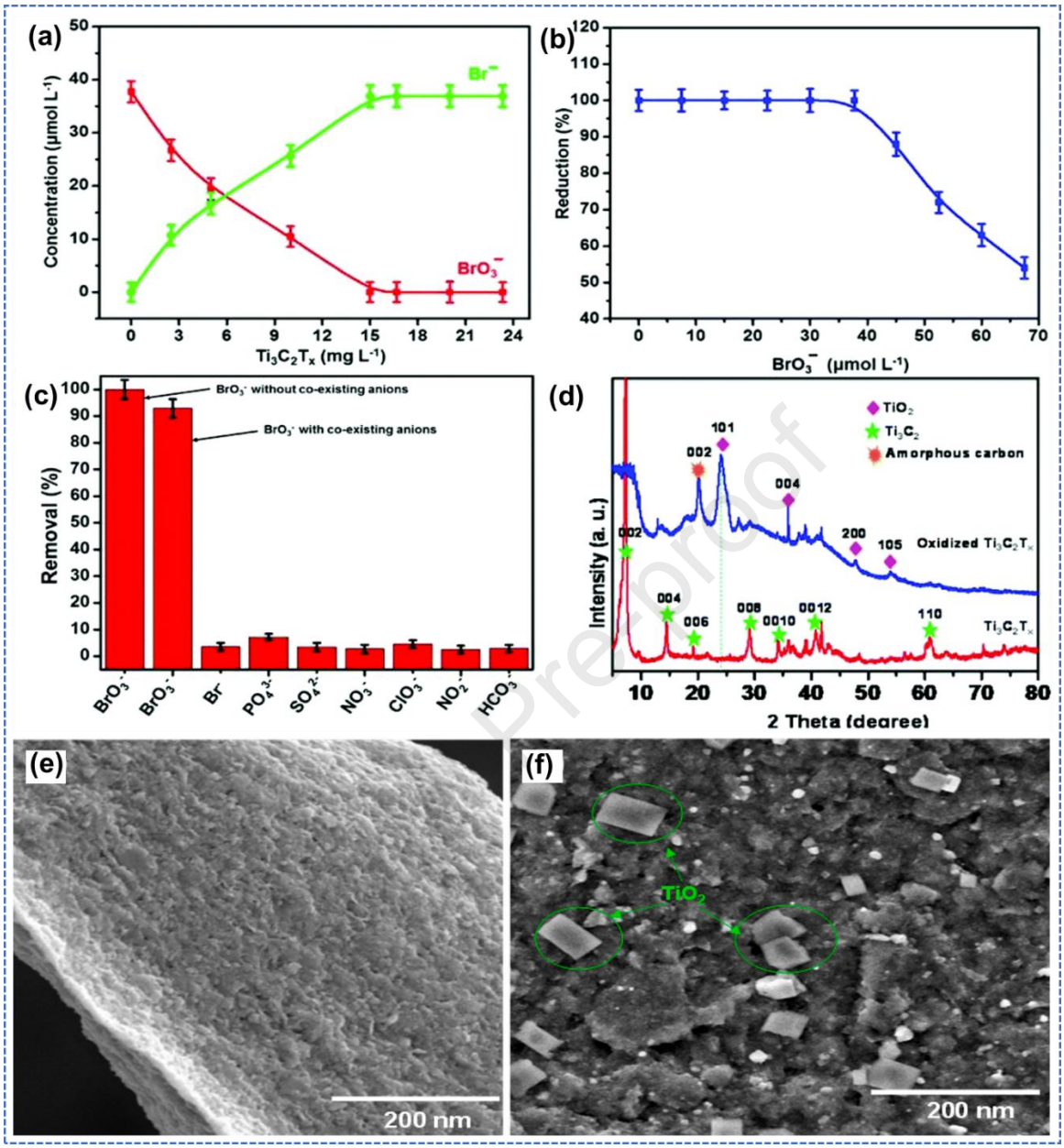

Fig. 17. (a) Impact of the absorption of $Ti_3C_2T_x$ upon the conversion of BrO_3^-. **(b)** Conversion (%) of various bromate concentrations utilizing 15 mg L^{-1} $Ti_3C_2T_x$ on pH 7 and 25 °C. **(c)** Influence of synchronized negative ion upon the decrease of bromate through $Ti_3C_2T_x$. **(d)** XRD graph of $Ti_3C_2T_x$ previously and afterward the modification of BrO_3^- to Br^-. SEM pictures of flakes $Ti_3C_2T_x$: **(e)** before modification of BrO_3^- and **(f)** after modification of BrO_3^-. Reprinted with permission from Ref. (Pandey et al., 2018a).

5.7. Bacterial pathogens degradation by MXene-based nanomaterials

2D $Ti_3C_2T_x$ has been newly investigated for utilization in water desalination/purifying films. A significant progress symbol toward any water processing membrane is the protection over biofouling. To confirm this and adequately recognize the well-being and ecological consequences of the novel 2D carbides, Kashif *et al*. (Rasool et al., 2016) studied the antiseptic characteristics of individual and multi-faceted $Ti_3C_2T_x$ MXene sheets into colloidal media. The antiseptic performance of $Ti_3C_2T_x$, including GO, both bacterial strains were used with distinct collections of GO below the corresponding laboratory circumstances. **Fig. 18(a)** Regular show antibacterial performance of $Ti_3C_2T_x$ MXene. **Fig. 18(b-c)** confirms the feasibility of each *Escherichia coli* (*E. coli*) and *B. subtilis* microbes under command, occupied as 100%, and revealed to 0-200 μg/mL of GO. There were significant variations within bacteria groups upon agar plates toward both bacterial forces, intimating that the $Ti_3C_2T_x$ MXene has a more potent antibacterial venture than GO within the laboratory setup. Unlike absorptions of $Ti_3C_2T_x$ used bacteria for 4 h, refined upon agar dishes, and assessed utilizing the microbe's numeration process. **Fig. 18(d-o)** exhibits the standard images of *E. coli* or *B. subtilis* bacteria groups after processing by different concentrations of bacteria. As observed from equal boards, the quantity of groups suggestively declines with the growing density of $Ti_3C_2T_x$. The achieved outcomes show the dose-based antimicrobic performance of $Ti_3C_2T_x$.

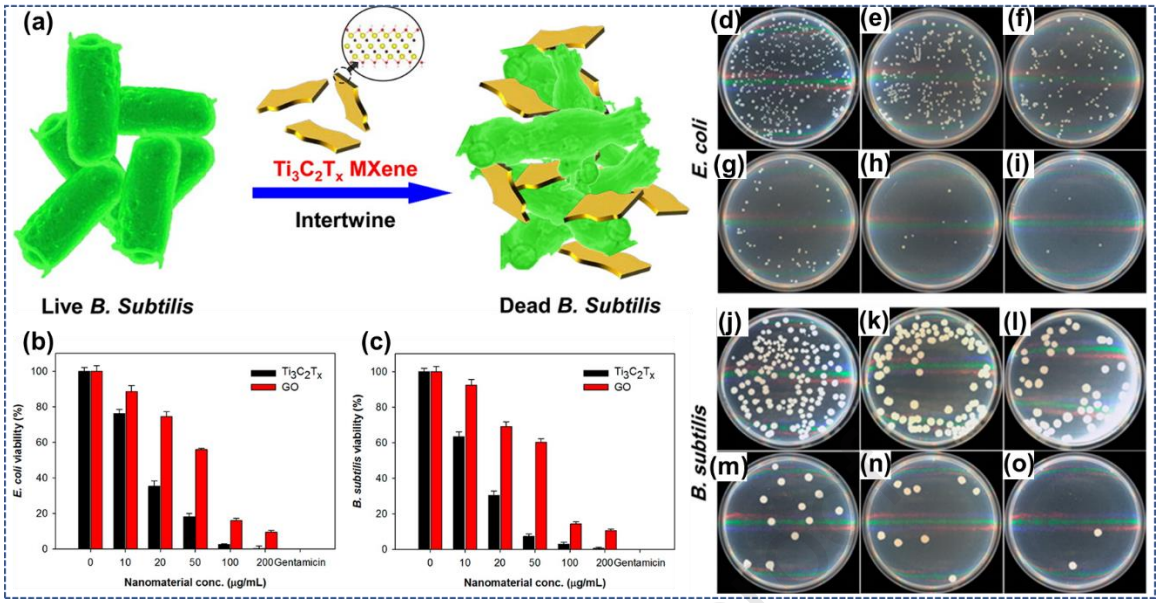

Fig. 18. (a) Systematic exhibition antibacterial action of $Ti_3C_2T_x$ MXene. Cell feasibility analyses of **(b)** *E. coli* and **(c)** *B. subtilis* used by $Ti_3C_{2T}x$and GO in aqueous solution. Microbial solution (10^7 CFU/mL) were produced beside distinct $Ti_3C_2T_x$ and GO absorptions (0-200 μg/mL) about 35 °C for 4 h at 150 rpm agitating pace. Concentration-based antiseptic performance of the $Ti_3C_2T_x$ in aqueous solution: Images of agar dishes over which *E. coli* (top sheet) and *B. subtilis* (base sheet) microbial cells were refined subsequent processing for 4 h by 0 to 200 μg/mL **(d-o)** of $Ti_3C_2T_x$, sequentially. Reprinted with permission from Ref. (Rasool et al., 2016).

Two common pathogenic microorganisms, *Staphylococcus aureus* (*S. aureus*) and *E. coli*, were taken to estimate the antiseptic activity of the substances. Following 10 min of NIR radiation, 200 ppm of $Bi_2S_3/Ti_3C_2T_x$-5 showed functional microbes-terminating capabilities around 99.86 and 99.92% versus *S. aureus* and *E. coli*, sequentially. The investigations were carried with feast dish, live/inert fluorescence discolouration (Jastrzębska et al., 2019; Lim et al., 2020). The absorptivity of the microbial cell film included through *ortho*-nitrophenyl-β-galactoside (ONPG) alkylation exhibited the antiseptic tool versus *S. aureus* and *E. coli*. As presented in **Fig. 20(a,b),** no notable development was recognized toward the optical denseness on 420 nm (OD_{420}) standards of

S. aureus and *E. coli* toward $Ti_3C_2T_x$ associated with the resistor assembly, showing consistent bacterial film penetrability.

Based upon the above stated in vitro outcomes and a rat injury pattern by *S. aureus* (1×10^8 CFU mL^{-1}) was developed to estimate the in vivo healing effectiveness amidst dressing, a 3 M wound bandaging, $Bi_2S_3/Ti_3C_2T_x$-5, and an essential assortment. The estimated measurable kin injury sections were exhibited within **Fig. 19(c)**; the injuries of the $Bi_2S_3/Ti_3C_2T_x$-5 group improved, showing a sharp scar healing inclination. Besides, hematoxylin and eosin (H&E) discolouration of scar tissues obtained at 2, 4, 8, and 12 d verified the remedial injury movement (**Fig. 19(d)**). Consequently, the antiseptic tool is sequentially shown within **Fig. 19(e)**. The improved $Bi_2S_3/Ti_3C_2T_x$ Schottky coupling generated more electrons and efficiently parted negative ion carrier and holes, inducing immutable loss to microbes. The photothermal impact of the specimens reduced the feasibility of the microorganisms. The synergetic influences of the ROS and the photothermal impact eliminated the bacteria quickly and efficiently (Li et al., 2021b).

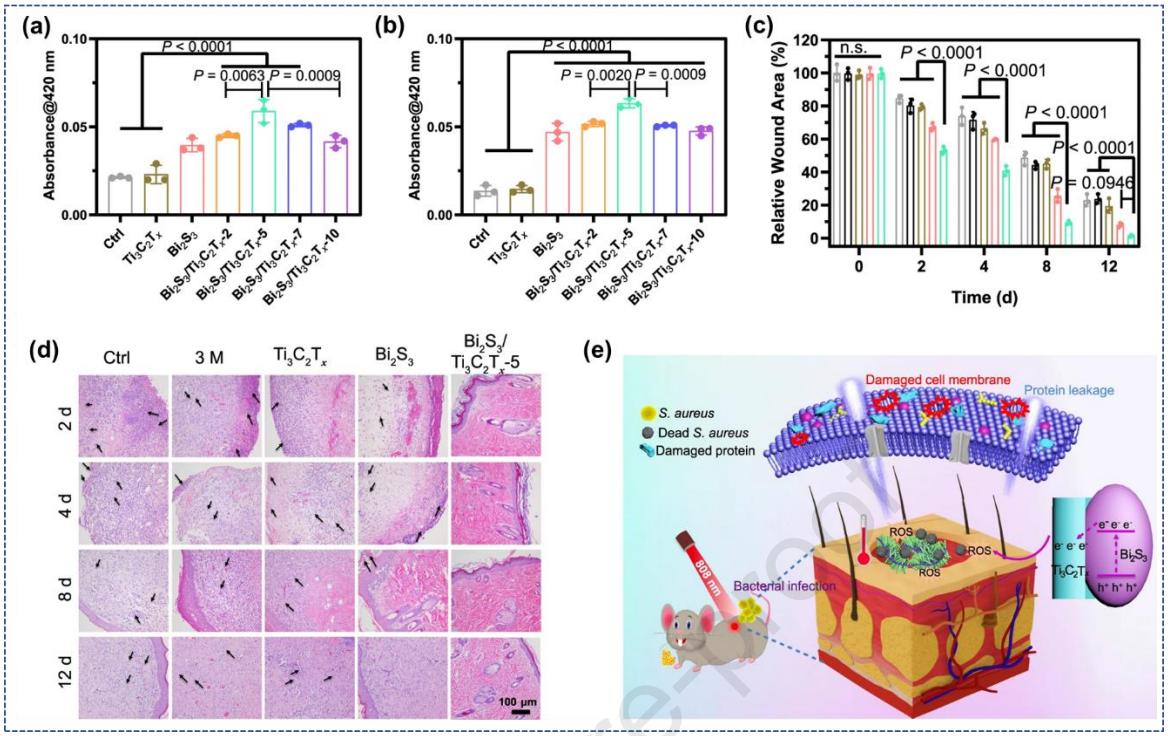

Fig. 19. ONPG alkylation of *S. aureus* (**a**) and *E. coli* (**b**) following 10 min lightning of different MBNs in vitro. (**c)** The Quantifiable determination of relevant injury section at 2, 4, 8, and 12 d of resistor, 3 M wound bandaging upon *S. aureus* (10 μL, 1 × 10^8 CFU/mL) to infectious injury remedial in vivo. Grey rings show the combination of control; black rings show the combination of 3 M, brown rings show the combination of $Ti_3C_2T_x$, pink rings show the combination of Bi_2S_3, and green rings show the combination $Bi_2S_3/Ti_3C_2T_x$-5. (**d**) Histologic pictures of injury muscle obtained at 2, 4, 8, and 12 d, including H&E discolouration. (**e)** The Graphic representation of $Bi_2S_3/Ti_3C_2T_x$ Schottky synergist and antiseptic tool description of $Bi_2S_3/Ti_3C_2T_x$ below 808 nm radiation. Reprinted with permission from Ref. (Li et al., 2021b).

6. Other applications of MXene-based nanomaterials

The novel transformable 2D in-layer nanostructure and controllable chemical arrangements support 2D MXenes with universal characteristics in profiting biomedical utilizations. These 2D multifunctional MBNs have been designed for theranostic applications, such as standard phototherapy of photothermal treatment (PTT),

photodynamic/chemo synergistic therapy, diagnostic imaging, antimicrobial, and biosensing (Lin et al., 2018).

The universal physicochemical effects of 2D nanofilms facilitate significant prospects for diagnostic imaging, signifying that they would work as contrast agents (CAs) to improve the diagnostic-imaging interpretation (Yang et al., 2013). Further, the universal applications of 2D nanomaterials towards therapeutics and diagnostic imaging would also be utilised as unique biosensing systems to detect biomacromolecules and bio-effects. Single-layer MoS2 nanofilms have been employed as biosensors for DNA detection based on their fluorescence-quenching solid performance (Zhu et al., 2013).

Different 2D nanomaterials have been investigated following various possible antibacterial actions. For example, after the accumulation of Zn-Ti layered double hydroxides (LDHs) to bacteria solution beneath visible light, the development of microbial species like *S. cerevisiae*, *S. aureus*, or *Escherichia coli* was significantly hindered because of the LDH dimension effect and generation of reactive oxygen species (ROS) by Ti^{3+} beneath visible rays (Zhao et al., 2013). Standard organic substances with good biocompatibility/biodegradation have been studied towards biomedical implementations. Inappropriately, their inadequate chemical/thermal durability and single functionality are the disadvantages restricting their clinical outcom (Song et al., 2017). Inorganic 2D MBNs exhibit fairly heightened clinical translation prospects, emanating from their intrinsic properties, for example, facile functionalization, tunable surface/structure and required biocompatibility.

7. Summary, challenges and outlook

In conclusion, MXene and MXene-related nanomaterials have appeared as upcoming competitors toward the adsorptive reduction of an assemblage of ecologically associated contaminants of water and sewer water. Targeted contaminating factors considered toward elimination involve organic colourants, poisonous heavy elements, pesticide residuals, antibiotics, and many more. MBNs are growing uninterruptedly to determine their probability within the field of wastewater disinfection and remedy. Given broader functionality, high surface area, and surface tunability, MBNs are considered to decrease inorganic contaminants through interfacial chemical conversion and sorption. In contrast, three different technologies, such as (i) exterior complexation and sorption (ii) catalytic initiation and extraction and (iii) radical's-dependent photocatalytic degeneration, are included within the replacement of organic pollutants. Though, significant consideration must be paid to designing and producing innovative laboratory-dependent MBNs with flexible surface chemistry, various TM ions, and strong characteristics to catch contaminants. The distinctive characteristics of MXene films induce them to promising nominees as alternates to noble metal substances for various electrochemical responses and wastewater treatment. This strategy outlines the novel outcome within the investigation of MXene and indicates the rapid development of the MXene analysis clusters. The results achieved into groundwork and characteristics, together with the uncovered application of MXene, produce a solid momentum for the most outlying outcome within the report and synthesis routes of these most delinquent 2D substances.

The effective elimination of different contaminants from the atmosphere is a hurdle, and the adsorption and catalytic degeneration methods are customarily considered the typical simple and efficient approaches. The quickly increasing interest toward practising MXene-

based substances concerning environmental applicability has been excited with the exciting findings of rare features and activity of GO-related nanocomposites, TM dichalcogenides (especially MoS_2), LDHs, etc. Their natural issues are also revealed, for example, the high price and hydrophobicity of Gr, the hydrophobicity of MoS_2 and the complexity of the large-range generation of single-layer MoS_2 with high-class, low resistance of LDHs in mixed suspensions. Though the efforts of researchers have mitigated these challenges, it is a hurdle to resolve them essentially.

Hence, additional studies are required to profoundly examine the utilization of MBNs in decreasing a large number of poisonous pollutants from identical wastewater specimens. Furthermore, a similar investigation should be imposed among MXenes and a series of different nano adsorbents, like GO, MOFs, CNTs, U; unquestionably, MBNs are expected to arrive quickly in the profitable business toward different utilization. Regarding strengthening results in many articles, it may be assumed that MBNs would be recognized as the next-generation competitors toward water purification.

Acknowledgement: The authors acknowledge the support from the Department of Chemistry and Research & Development Cell of Maharishi Markandeshwar (Deemed to be University), Mullana, Ambala, Haryana, India.

References:

Abbasi, N.M., Xiao, Y., Peng, L., Duo, Y., Wang, L., Zhang, L., Wang, B., Zhang, H., 2021. Recent Advancement for the Synthesis of MXene Derivatives and Their Sensing Protocol. Advanced Materials Technologies 6, 2001197.

Ahmed, F.E., Khalil, A., Hilal, N., 2021. Emerging desalination technologies: Current status, challenges and future trends. Desalination 517, 115183.

Al-Hamadani, Y.A.J., Jun, B.-M., Yoon, M., Taheri-Qazvini, N., Snyder, S.A., Jang, M., Heo, J., Yoon, Y., 2020. Applications of MXene-based membranes in water purification: A review. Chemosphere 254, 126821.

Alhabeb, M., Maleski, K., Anasori, B., Lelyukh, P., Clark, L., Sin, S., Gogotsi, Y., 2017. Guidelines for Synthesis and Processing of Two-Dimensional Titanium Carbide (Ti3C2Tx MXene). Chemistry of Materials 29, 7633-7644.

Anasori, B., Lukatskaya, M.R., Gogotsi, Y., 2017. 2D metal carbides and nitrides (MXenes) for energy storage. Nature Reviews Materials 2, 16098.

Augustyn, V., Gogotsi, Y., 2017. 2D Materials with Nanoconfined Fluids for Electrochemical Energy Storage. Joule 1, 443-452.

Bai, S., Yang, M., Jiang, J., He, X., Zou, J., Xiong, Z., Liao, G., Liu, S., 2021. Recent advances of MXenes as electrocatalysts for hydrogen evolution reaction. npj 2D Materials and Applications 5, 78.

Bai, Y., Zhou, K., Srikanth, N., Pang, J.H.L., He, X., Wang, R., 2016. Dependence of elastic and optical properties on surface terminated groups in two-dimensional MXene monolayers: a first-principles study. RSC Advances 6, 35731-35739.

Bao, W., Tang, X., Guo, X., Choi, S., Wang, C., Gogotsi, Y., Wang, G., 2018. Porous Cryo-Dried MXene for Efficient Capacitive Deionization. Joule 2, 778-787.

Barsoum, M.W., Radovic, M., 2011. Elastic and Mechanical Properties of the MAX Phases. Annual Review of Materials Research 41, 195-227.

Berkani, M., Smaali, A., Almomani, F., Vasseghian, Y., 2022. Recent advances in MXene-based nanomaterials for desalination at water interfaces. Environmental Research 203, 111845.

Bharath, G., Arora, N., Hai, A., Banat, F., Savariraj, D., Taher, H., Mangalaraja, R.V., 2020. Synthesis of hierarchical Mn3O4 nanowires on reduced graphene oxide nanoarchitecture as effective pseudocapacitive electrodes for capacitive desalination application. Electrochimica Acta 337, 135668.

Borysiuk, V.N., Mochalin, V.N., Gogotsi, Y., 2015. Molecular dynamic study of the mechanical properties of two-dimensional titanium carbides Tin+1Cn (MXenes). Nanotechnology 26, 265705.

Cai, T., Wang, L., Liu, Y., Zhang, S., Dong, W., Chen, H., Yi, X., Yuan, J., Xia, X., Liu, C., Luo, S., 2018. Ag3PO4/Ti3C2 MXene interface materials as a Schottky catalyst with enhanced photocatalytic activities and anti-photocorrosion performance. Applied Catalysis B: Environmental 239, 545-554.

Cao, Y., Fang, Y., Lei, X., Tan, B., Hu, X., Liu, B., Chen, Q., 2020. Fabrication of novel CuFe2O4/MXene hierarchical heterostructures for enhanced photocatalytic degradation of sulfonamides under visible light. Journal of Hazardous Materials 387, 122021.

Chandel, N., Sharma, K., Sudhaik, A., Raizada, P., Hosseini-Bandegharaei, A., Thakur, V.K., Singh, P., 2020. Magnetically separable ZnO/ZnFe2O4 and ZnO/CoFe2O4 photocatalysts supported onto nitrogen doped graphene for photocatalytic degradation of toxic dyes. Arabian Journal of Chemistry 13, 4324–4340.

Chen, C., Boota, M., Urbankowski, P., Anasori, B., Miao, L., Jiang, J., Gogotsi, Y., 2018. Effect of glycine functionalization of 2D titanium carbide (MXene) on charge storage. Journal of Materials Chemistry A 6, 4617-4622.

Chen, J., Huang, Q., Huang, H., Mao, L., Liu, M., Zhang, X., Wei, Y., 2020. Recent progress and advances in the environmental applications of MXene related materials. Nanoscale 12, 3574-3592.

Chen, Y., Xie, X., Xin, X., Tang, Z.-R., Xu, Y.-J., 2019. Ti3C2Tx-Based Three-Dimensional Hydrogel by a Graphene Oxide-Assisted Self-Convergence Process for Enhanced Photoredox Catalysis. ACS Nano 13, 295-304.

Chen, Z., Xu, X., Ding, Z., Wang, K., Sun, X., Lu, T., Konarova, M., Eguchi, M., Shapter, J.G., Pan, L., Yamauchi, Y., 2021. Ti3C2 MXenes-derived NaTi2(PO4)3/MXene nanohybrid for fast and efficient hybrid capacitive deionization performance. Chemical Engineering Journal 407, 127148.

Couly, C., Alhabeb, M., Van Aken, K.L., Kurra, N., Gomes, L., Navarro-Suárez, A.M., Anasori, B., Alshareef, H.N., Gogotsi, Y., 2018. Asymmetric Flexible MXene-Reduced Graphene Oxide Micro-Supercapacitor. Advanced Electronic Materials 4, 1700339.

Cui, C., Guo, R., Xiao, H., Ren, E., Song, Q., Xiang, C., Lai, X., Lan, J., Jiang, S., 2020. Bi2WO6/Nb2CTx MXene hybrid nanosheets with enhanced visible-light-driven photocatalytic activity for organic pollutants degradation. Applied Surface Science 505, 144595.

Cui, L., Wang, Y., Gao, L., Hu, L., Yan, L., Wei, Q., Du, B., 2015. EDTA functionalized magnetic graphene oxide for removal of Pb(II), Hg(II) and Cu(II) in water treatment: Adsorption mechanism and separation property. Chemical Engineering Journal 281, 1-10.

Ding, X., Li, C., Wang, L., Feng, L., Han, D., Wang, W., 2019. Fabrication of hierarchical g-C3N4/MXene-AgNPs nanocomposites with enhanced photocatalytic performances. Materials Letters 247, 174-177.

Fard, L.A., Ojani, R., Raoof, J.B., Zare, E.N., Lakouraj, M.M., 2017. Poly (pyrrole-co-aniline) hollow nanosphere supported Pd nanoflowers as high-performance catalyst for methanol electrooxidation in alkaline media. Energy 127, 419-427.

Feng, J., Yang, J., Shen, Y., Deng, W., Chen, W., Ma, Y., Chen, Z., Dong, S., 2021. Mesoporous silica nanoparticles prepared via a one-pot method for controlled release of abamectin: Properties and applications. Microporous and Mesoporous Materials 311, 110688.

Fu, L., Yan, Z., Zhao, Q., Yang, H., 2018. Novel 2D Nanosheets with Potential Applications in Heavy Metal Purification: A Review. Advanced Materials Interfaces 5, 1801094.

Gao, Y., Wang, L., Zhou, A., Li, Z., Chen, J., Bala, H., Hu, Q., Cao, X., 2015. Hydrothermal synthesis of TiO2/Ti3C2 nanocomposites with enhanced photocatalytic activity. Materials Letters 150, 62-64.

Ghidiu, M., Lukatskaya, M.R., Zhao, M.-Q., Gogotsi, Y., Barsoum, M.W., 2014. Conductive two-dimensional titanium carbide 'clay' with high volumetric capacitance. Nature 516, 78-81.

Gogotsi, Y., 2015. Transition metal carbides go 2D. Nature Materials 14, 1079-1080.

Gu, P., Xing, J., Wen, T., Zhang, R., Wang, J., Zhao, G., Hayat, T., Ai, Y., Lin, Z., Wang, X., 2018. Experimental and theoretical calculation investigation on efficient Pb(ii) adsorption on etched Ti3AlC2 nanofibers and nanosheets. Environmental Science: Nano 5, 946-955.

Guo, L., Wang, X., Leong, Z.Y., Mo, R., Sun, L., Yang, H.Y., 2018. Ar plasma modification of 2D MXene Ti3C2Tx nanosheets for efficient capacitive desalination. FlatChem 8, 17-24.

Guo, Z., Zhou, J., Si, C., Sun, Z., 2015. Flexible two-dimensional Tin+1Cn (n = 1, 2 and 3) and their functionalized MXenes predicted by density functional theories. Physical Chemistry Chemical Physics 17, 15348-15354.

Han, R., Wu, P., 2019. High-performance graphene oxide nanofiltration membrane with continuous nanochannels prepared by the in situ oxidation of MXene. Journal of Materials Chemistry A 7, 6475-6481.

Hao, L., Gong, L., Chen, L., Guan, M., Zhou, H., Qiu, S., Wen, H., Chen, H., Zhou, X., Akbulut, M., 2020. Composite pesticide nanocarriers involving functionalized boron nitride nanoplatelets for pH-responsive release and enhanced UV stability. Chemical Engineering Journal 396, 125233.
Horlait, D., Middleburgh, S.C., Chroneos, A., Lee, W.E., 2016. Synthesis and DFT investigation of new bismuth-containing MAX phases. Scientific Reports 6, 18829.
Hua, M., Zhang, S., Pan, B., Zhang, W., Lv, L., Zhang, Q., 2012. Heavy metal removal from water/wastewater by nanosized metal oxides: A review. Journal of Hazardous Materials 211-212, 317-331.
Huang, G., Deng, Y., Zhang, Y., Feng, P., Xu, C., Fu, L., Lin, B., 2021. Study on long-term pest control and stability of double-layer pesticide carrier in indoor and outdoor environment. Chemical Engineering Journal 403, 126342.
Ihsanullah, Abbas, A., Al-Amer, A.M., Laoui, T., Al-Marri, M.J., Nasser, M.S., Khraisheh, M., Atieh, M.A., 2016. Heavy metal removal from aqueous solution by advanced carbon nanotubes: Critical review of adsorption applications. Separation and Purification Technology 157, 141-161.
Islam, A., Teo, S.H., Taufiq-Yap, Y.H., Ng, C.H., Vo, D.-V.N., Ibrahim, M.L., Hasan, M.M., Khan, M.A.R., Nur, A.S.M., Awual, M.R., 2021. Step towards the sustainable toxic dyes removal and recycling from aqueous solution- A comprehensive review. Resources, Conservation and Recycling 175, 105849.
Jaffari, Z.H., Abuabdou, S.M.A., Ng, D.-Q., Bashir, M.J.K., 2021. Insight into two-dimensional MXenes for environmental applications: Recent progress, challenges, and prospects. FlatChem 28, 100256.
Jang, J., Shahzad, A., Woo, S.H., Lee, D.S., 2020. Magnetic Ti3C2Tx (Mxene) for diclofenac degradation via the ultraviolet/chlorine advanced oxidation process. Environmental Research 182, 108990.
Jasper, J.T., Yang, Y., Hoffmann, M.R., 2017. Toxic Byproduct Formation during Electrochemical Treatment of Latrine Wastewater. Environmental Science & Technology 51, 7111-7119.
Jastrzębska, A.M., Karwowska, E., Wojciechowski, T., Ziemkowska, W., Rozmysłowska, A., Chlubny, L., Olszyna, A., 2019. The Atomic Structure of Ti2C and Ti3C2 MXenes is Responsible for Their Antibacterial Activity Toward E. coli Bacteria. Journal of Materials Engineering and Performance 28, 1272-1277.
Jiang, X., Kuklin, A.V., Baev, A., Ge, Y., Ågren, H., Zhang, H., Prasad, P.N., 2020. Two-dimensional MXenes: From morphological to optical, electric, and magnetic properties and applications. Physics Reports 848, 1-58.
Jun, B.-M., Her, N., Park, C.M., Yoon, Y., 2020a. Effective removal of Pb(ii) from synthetic wastewater using Ti3C2Tx MXene. Environmental Science: Water Research & Technology 6, 173-180.
Jun, B.-M., Park, C.M., Heo, J., Yoon, Y., 2020b. Adsorption of Ba2+ and Sr2+ on Ti3C2Tx MXene in model fracking wastewater. Journal of Environmental Management 256, 109940.
Khazaei, M., Arai, M., Sasaki, T., Ranjbar, A., Liang, Y., Yunoki, S., 2015. OH-terminated two-dimensional transition metal carbides and nitrides as ultralow work function materials. Physical Review B 92, 075411.
Kumar, J.A., Prakash, P., Krithiga, T., Amarnath, D.J., Premkumar, J., Rajamohan, N., Vasseghian, Y., Saravanan, P., Rajasimman, M., 2022. Methods of synthesis, characteristics, and environmental applications of MXene: A comprehensive review. Chemosphere 286, 131607.
Li, G., Wyatt, B.C., Song, F., Yu, C., Wu, Z., Xie, X., Anasori, B., Zhang, N., 2021a. 2D Titanium Carbide (MXene) Based Films: Expanding the Frontier of Functional Film Materials. Advanced Functional Materials n/a, 2105043.

Li, J., Li, Z., Liu, X., Li, C., Zheng, Y., Yeung, K.W.K., Cui, Z., Liang, Y., Zhu, S., Hu, W., Qi, Y., Zhang, T., Wang, X., Wu, S., 2021b. Interfacial engineering of Bi2S3/Ti3C2Tx MXene based on work function for rapid photo-excited bacteria-killing. Nature Communications 12, 1224.

Li, J., Wang, S., Du, Y., Liao, W., 2018a. Enhanced photocatalytic performance of TiO2@C nanosheets derived from two-dimensional Ti2CTx. Ceramics International 44, 7042-7046.

Li, Q., Li, Y., Zeng, W., 2021c. Preparation and Application of 2D MXene-Based Gas Sensors: A Review. Chemosensors 9.

Li, T., Yao, L., Liu, Q., Gu, J., Luo, R., Li, J., Yan, X., Wang, W., Liu, P., Chen, B., Zhang, W., Abbas, W., Naz, R., Zhang, D., 2018b. Fluorine-Free Synthesis of High-Purity Ti3C2Tx (T=OH, O) via Alkali Treatment. Angewandte Chemie International Edition 57, 6115-6119.

Li, X., Dong, H., Wang, Z., Han, F., 2019. Set-Membership Filtering for State-Saturated Systems With Mixed Time-Delays Under Weighted Try-Once-Discard Protocol. IEEE Transactions on Circuits and Systems II: Express Briefs 66, 312-316.

Lim, G.P., Soon, C.F., Morsin, M., Ahmad, M.K., Nayan, N., Tee, K.S., 2020. Synthesis, characterization and antifungal property of Ti3C2Tx MXene nanosheets. Ceramics International 46, 20306-20312.

Lin, H., Wang, Y., Gao, S., Chen, Y., Shi, J., 2018. Theranostic 2D Tantalum Carbide (MXene). Advanced Materials 30, 1703284.

Ling, Z., Ren, C.E., Zhao, M.-Q., Yang, J., Giammarco, J.M., Qiu, J., Barsoum, M.W., Gogotsi, Y., 2014. Flexible and conductive MXene films and nanocomposites with high capacitance. Proceedings of the National Academy of Sciences 111, 16676.

Liu, F., Zhou, J., Wang, S., Wang, B., Shen, C., Wang, L., Hu, Q., Huang, Q., Zhou, A., 2017a. Preparation of High-Purity V2C MXene and Electrochemical Properties as Li-Ion Batteries. Journal of The Electrochemical Society 164, A709-A713.

Liu, G., Shen, J., Liu, Q., Liu, G., Xiong, J., Yang, J., Jin, W., 2018. Ultrathin two-dimensional MXene membrane for pervaporation desalination. Journal of Membrane Science 548, 548-558.

Liu, N., Lu, N., Su, Y., Wang, P., Quan, X., 2019a. Fabrication of g-C3N4/Ti3C2 composite and its visible-light photocatalytic capability for ciprofloxacin degradation. Separation and Purification Technology 211, 782-789.

Liu, N., Lu, N., Yu, H., Chen, S., Quan, X., 2020. Efficient day-night photocatalysis performance of 2D/2D Ti3C2/Porous g-C3N4 nanolayers composite and its application in the degradation of organic pollutants. Chemosphere 246, 125760.

Liu, Q., Tan, X., Wang, S., Ma, F., Znad, H., Shen, Z., Liu, L., Liu, S., 2019b. MXene as a non-metal charge mediator in 2D layered CdS@Ti3C2@TiO2 composites with superior Z-scheme visible light-driven photocatalytic activity. Environmental Science: Nano 6, 3158-3169.

Liu, T., Zhou, T., Yao, Y., Zhang, F., Liu, L., Liu, Y., Leng, J., 2017b. Stimulus methods of multi-functional shape memory polymer nanocomposites: A review. Composites Part A: Applied Science and Manufacturing 100, 20-30.

Liu, Y., Xiao, H., Goddard, W.A., 2016a. Schottky-Barrier-Free Contacts with Two-Dimensional Semiconductors by Surface-Engineered MXenes. Journal of the American Chemical Society 138, 15853-15856.

Liu, Z., Xu, C., Kang, N., Wang, L., Jiang, Y., Du, J., Liu, Y., Ma, X.-L., Cheng, H.-M., Ren, W., 2016b. Unique Domain Structure of Two-Dimensional α-Mo2C Superconducting Crystals. Nano Letters 16, 4243-4250.

Long, Q., Zhao, S., Chen, J., Zhang, Z., Qi, G., Liu, Z.-Q., 2021. Self-assembly enabled nano-intercalation for stable high-performance MXene membranes. Journal of Membrane Science 635, 119464.

Lu, L., Yang, Q., Xu, Q., Sun, Y., Tang, S., Tang, X., Liang, H., Yu, Y., 2021a. Two-dimensional materials beyond graphene for the detection and removal of antibiotics: A critical review. Critical Reviews in Environmental Science and Technology, 1-32.
Lu, Y., Zhang, S., He, M., Wei, L., Chen, Y., Liu, R., 2021b. 3D cross-linked graphene or/and MXene based nanomaterials for electromagnetic wave absorbing and shielding. Carbon 178, 413-435.
Lukatskaya Maria, R., Mashtalir, O., Ren Chang, E., Dall'Agnese, Y., Rozier, P., Taberna Pierre, L., Naguib, M., Simon, P., Barsoum Michel, W., Gogotsi, Y., 2013. Cation Intercalation and High Volumetric Capacitance of Two-Dimensional Titanium Carbide. Science 341, 1502-1505.
Lukatskaya, M.R., Kota, S., Lin, Z., Zhao, M.-Q., Shpigel, N., Levi, M.D., Halim, J., Taberna, P.-L., Barsoum, M.W., Simon, P., Gogotsi, Y., 2017. Ultra-high-rate pseudocapacitive energy storage in two-dimensional transition metal carbides. Nature Energy 2, 17105.
Luo, S., Wang, R., Yin, J., Jiao, T., Chen, K., Zou, G., Zhang, L., Zhou, J., Zhang, L., Peng, Q., 2019. Preparation and Dye Degradation Performances of Self-Assembled MXene-Co3O4 Nanocomposites Synthesized via Solvothermal Approach. ACS Omega 4, 3946-3953.
Ma, J., Cheng, Y., Wang, L., Dai, X., Yu, F., 2020. Free-standing Ti3C2Tx MXene film as binder-free electrode in capacitive deionization with an ultrahigh desalination capacity. Chemical Engineering Journal 384, 123329.
Malaki, M., Maleki, A., Varma, R.S., 2019. MXenes and ultrasonication. Journal of Materials Chemistry A 7, 10843-10857.
Maleski, K., Mochalin, V.N., Gogotsi, Y., 2017. Dispersions of Two-Dimensional Titanium Carbide MXene in Organic Solvents. Chemistry of Materials 29, 1632-1640.
Martinez, J.L., 2009. Environmental pollution by antibiotics and by antibiotic resistance determinants. Environmental Pollution 157, 2893-2902.
Mashtalir, O., Cook, K.M., Mochalin, V.N., Crowe, M., Barsoum, M.W., Gogotsi, Y., 2014. Dye adsorption and decomposition on two-dimensional titanium carbide in aqueous media. Journal of Materials Chemistry A 2, 14334-14338.
Mashtalir, O., Naguib, M., Mochalin, V.N., Dall'Agnese, Y., Heon, M., Barsoum, M.W., Gogotsi, Y., 2013. Intercalation and delamination of layered carbides and carbonitrides. Nature Communications 4, 1716.
Mazari, S.A., Ali, E., Abro, R., Khan, F.S.A., Ahmed, I., Ahmed, M., Nizamuddin, S., Siddiqui, T.H., Hossain, N., Mubarak, N.M., Shah, A., 2021. Nanomaterials: Applications, waste-handling, environmental toxicities, and future challenges – A review. Journal of Environmental Chemical Engineering 9, 105028.
Meng, F., Seredych, M., Chen, C., Gura, V., Mikhalovsky, S., Sandeman, S., Ingavle, G., Ozulumba, T., Miao, L., Anasori, B., Gogotsi, Y., 2018. MXene Sorbents for Removal of Urea from Dialysate: A Step toward the Wearable Artificial Kidney. ACS Nano 12, 10518-10528.
Naguib, M., Barsoum, M.W., Gogotsi, Y., 2021. Ten Years of Progress in the Synthesis and Development of MXenes. Advanced Materials 33, 2103393.
Naguib, M., Kurtoglu, M., Presser, V., Lu, J., Niu, J., Heon, M., Hultman, L., Gogotsi, Y., Barsoum, M.W., 2011. Two-Dimensional Nanocrystals Produced by Exfoliation of Ti3AlC2. Advanced Materials 23, 4248-4253.
Osti, N.C., Naguib, M., Ostadhossein, A., Xie, Y., Kent, P.R.C., Dyatkin, B., Rother, G., Heller, W.T., van Duin, A.C.T., Gogotsi, Y., Mamontov, E., 2016. Effect of Metal Ion Intercalation on the Structure of MXene and Water Dynamics on its Internal Surfaces. ACS Applied Materials & Interfaces 8, 8859-8863.
Pandey, R.P., Rasool, K., Abdul Rasheed, P., Mahmoud, K.A., 2018a. Reductive Sequestration of Toxic Bromate from Drinking Water using Lamellar Two-Dimensional Ti3C2TX (MXene). ACS Sustainable Chemistry & Engineering 6, 7910-7917.

Pandey, R.P., Rasool, K., Madhavan, V.E., Aïssa, B., Gogotsi, Y., Mahmoud, K.A., 2018b. Ultrahigh-flux and fouling-resistant membranes based on layered silver/MXene (Ti3C2Tx) nanosheets. Journal of Materials Chemistry A 6, 3522-3533.
Patial, S., Raizada, P., Hasija, V., Singh, P., Thakur, V.K., Nguyen, V.-H., 2021. Recent advances in photocatalytic multivariate metal organic frameworks-based nanostructures toward renewable energy and the removal of environmental pollutants. Materials Today Energy 19, 100589.
Pang, J., Mendes, R.G., Bachmatiuk, A., Zhao, L., Ta, H.Q., Gemming, T., Liu, H., Liu, Z., Rummeli, M.H., 2019. Applications of 2D MXenes in energy conversion and storage systems. Chemical Society Reviews 48, 72-133.
Peng, Q., Guo, J., Zhang, Q., Xiang, J., Liu, B., Zhou, A., Liu, R., Tian, Y., 2014. Unique Lead Adsorption Behavior of Activated Hydroxyl Group in Two-Dimensional Titanium Carbide. Journal of the American Chemical Society 136, 4113-4116.
Ranjith, K.S., Ezhil Vilian, A.T., Ghoreishian, S.M., Umapathi, R., Hwang, S.-K., Oh, C.W., Huh, Y.S., Han, Y.-K., 2022. Hybridized 1D–2D MnMoO4–MXene nanocomposites as high-performing electrochemical sensing platform for the sensitive detection of dihydroxybenzene isomers in wastewater samples. Journal of Hazardous Materials 421, 126775.
Ranjith, K.S., Vilian, A.T.E., Ghoreishian, S.M., Umapathi, R., Huh, Y.S., Han, Y.-K., 2021. An ultrasensitive electrochemical sensing platform for rapid detection of rutin with a hybridized 2D-1D MXene-FeWO4 nanocomposite. Sensors and Actuators B: Chemical 344, 130202.
Rasheed, T., Kausar, F., Rizwan, K., Adeel, M., Sher, F., Alwadai, N., Alshammari, F.H., 2022. Two dimensional MXenes as emerging paradigm for adsorptive removal of toxic metallic pollutants from wastewater. Chemosphere 287, 132319.
Rasool, K., Helal, M., Ali, A., Ren, C.E., Gogotsi, Y., Mahmoud, K.A., 2016. Antibacterial Activity of Ti3C2Tx MXene. ACS Nano 10, 3674-3684.
Rathi, B.S., Kumar, P.S., Vo, D.-V.N., 2021. Critical review on hazardous pollutants in water environment: Occurrence, monitoring, fate, removal technologies and risk assessment. Science of The Total Environment 797, 149134.
Raizada, P., Thakur, P., Sudhaik, A., Singh, P., Thakur, V.K., Hosseini-Bandegharaei, A., 2020. Fabrication of dual Z-scheme photocatalyst via coupling of BiOBr/Ag/AgCl heterojunction with P and S co-doped g-C3N4 for efficient phenol degradation. Arabian Journal of Chemistry 13, 4538–4552.
Rana, Ashvinder Kumar, Frollini, E., Thakur, V.K., 2021. Cellulose nanocrystals: Pretreatments, preparation strategies, and surface functionalization. International Journal of Biological Macromolecules 182, 1554–1581.
Rana, Ashvinder K., Gupta, V.K., Saini, A.K., Voicu, S.I., Abdellattifaand, M.H., Thakur, V.K., 2021a. Water desalination using nanocelluloses/cellulose derivatives based membranes for sustainable future. Desalination 520, 115359.
Rana, Ashvinder K., Mishra, Y.K., Gupta, V.K., Thakur, V.K., 2021b. Sustainable materials in the removal of pesticides from contaminated water: Perspective on macro to nanoscale cellulose. Science of The Total Environment 797, 149129.
Rehman, M.S.U., Rashid, N., Ashfaq, M., Saif, A., Ahmad, N., Han, J.-I., 2015. Global risk of pharmaceutical contamination from highly populated developing countries. Chemosphere 138, 1045-1055.
Ren, C.E., Zhao, M.-Q., Makaryan, T., Halim, J., Boota, M., Kota, S., Anasori, B., Barsoum, M.W., Gogotsi, Y., 2016. Porous Two-Dimensional Transition Metal Carbide (MXene) Flakes for High-Performance Li-Ion Storage. ChemElectroChem 3, 689-693.

Robinson, T., McMullan, G., Marchant, R., Nigam, P., 2001. Remediation of dyes in textile effluent: a critical review on current treatment technologies with a proposed alternative. Bioresource Technology 77, 247-255.

Sharma, B., Thakur, S., Mamba, G., Prateek, Gupta, R.K., Gupta, V.K., Thakur, V.K., 2020. Titania modified gum tragacanth based hydrogel nanocomposite for water remediation. Journal of Environmental Chemical Engineering 104608.

Siwal, S.S., Zhang, Q., Devi, N., Saini, A.K., Saini, V., Pareek, B., Gaidukovs, S., Thakur, V.K., 2021. Recovery processes of sustainable energy using different biomass and wastes. Renewable and Sustainable Energy Reviews 150, 111483.

Samarjeet, S., Sarit, G., Debkumar, N., Nishu, D., Venkata, K.P., Rasmita, B., Kaushik, M., 2017. Synergistic effect of graphene oxide on the methanol oxidation for fuel cell application. Materials Research Express 4, 095306.

Schultz, T., Frey, N.C., Hantanasirisakul, K., Park, S., May, S.J., Shenoy, V.B., Gogotsi, Y., Koch, N., 2019. Surface Termination Dependent Work Function and Electronic Properties of Ti3C2Tx MXene. Chemistry of Materials 31, 6590-6597.

Shahzad, A., Nawaz, M., Moztahida, M., Jang, J., Tahir, K., Kim, J., Lim, Y., Vassiliadis, V.S., Woo, S.H., Lee, D.S., 2019. Ti3C2Tx MXene core-shell spheres for ultrahigh removal of mercuric ions. Chemical Engineering Journal 368, 400-408.

Shahzad, A., Rasool, K., Miran, W., Nawaz, M., Jang, J., Mahmoud, K.A., Lee, D.S., 2018. Mercuric ion capturing by recoverable titanium carbide magnetic nanocomposite. Journal of Hazardous Materials 344, 811-818.

Shao, L., Chen, G.Q., 2013. Water Footprint Assessment for Wastewater Treatment: Method, Indicator, and Application. Environmental Science & Technology 47, 7787-7794.

Shen, J., Shen, J., Zhang, W., Yu, X., Tang, H., Zhang, M., Zulfiqar, Liu, Q., 2019. Built-in electric field induced CeO2/Ti3C2-MXene Schottky-junction for coupled photocatalytic tetracycline degradation and CO2 reduction. Ceramics International 45, 24146-24153.

Shi, X., Wang, P., Lan, L., Jia, S., Wei, Z., 2019. Construction of BiOBrxI1−x/MXene Ti3C2Tx composite for improved photocatalytic degradability. Journal of Materials Science: Materials in Electronics 30, 19804-19812.

Shi, Y., Sun, M., Liu, C., Fu, L., Lv, Y., Feng, Y., Huang, P., Yang, F., Song, P., Liu, M., 2022. Lightweight, amphipathic and fire-resistant prGO/MXene spherical beads for rapid elimination of hazardous chemicals. Journal of Hazardous Materials 423, 127069.

Siwal, S., Devi, N., Perla, V., Barik, R., Ghosh, S., Mallick, K., 2018. The influencing role of oxophilicity and surface area of the catalyst for electrochemical methanol oxidation reaction: a case study. Materials Research Innovations, 1-8.

Siwal, S., Devi, N., Perla, V.K., Ghosh, S.K., Mallick, K., 2019a. Promotional role of gold in electrochemical methanol oxidation. Catalysis, Structure & Reactivity 5, 1-9.

Siwal, S.S., Saini, A.K., Rarotra, S., Zhang, Q., Thakur, V.K., 2021a. Recent advancements in transparent carbon nanotube films: chemistry and imminent challenges. Journal of Nanostructure in Chemistry.

Siwal, S.S., Thakur, V.K., Zhang, Q., 2021b. 12 - Bio-electrochemical systems for sustainable energy production and environmental prospects. in: Hussain, C.M., Shukla, S.K., Joshi, G.M. (Eds.). Functionalized Nanomaterials Based Devices for Environmental Applications. Elsevier, pp. 275-301.

Siwal, S.S., Yang, W., Zhang, Q., 2020a. Recent progress of precious-metal-free electrocatalysts for efficient water oxidation in acidic media. Journal of Energy Chemistry 51, 113-133.

Siwal, S.S., Zhang, Q., Devi, N., Thakur, K.V., 2020b. Carbon-Based Polymer Nanocomposite for High-Performance Energy Storage Applications. Polymers 12.
Siwal, S.S., Zhang, Q., Saini, A.K., Gupta, V.K., Roberts, D., Saini, V., Coulon, F., Pareek, B., Thakur, V.K., 2021c. Recent advances in bio-electrochemical system analysis in biorefineries. Journal of Environmental Chemical Engineering 9, 105982.
Siwal, S.S., Zhang, Q., Sun, C., Thakur, V.K., 2019b. Graphitic Carbon Nitride Doped Copper–Manganese Alloy as High–Performance Electrode Material in Supercapacitor for Energy Storage. Nanomaterials 10.
Song, P., Liu, B., Qiu, H., Shi, X., Cao, D., Gu, J., 2021a. MXenes for polymer matrix electromagnetic interference shielding composites: A review. Composites Communications 24, 100653.
Song, S., Jiang, X., Shen, H., Wu, W., Shi, Q., Wan, M., Zhang, J., Mo, H., Shen, J., 2021b. MXene (Ti3C2) Based Pesticide Delivery System for Sustained Release and Enhanced Pest Control. ACS Applied Bio Materials 4, 6912-6923.
Song, Z., Han, Z., Lv, S., Chen, C., Chen, L., Yin, L., Cheng, J., 2017. Synthetic polypeptides: from polymer design to supramolecular assembly and biomedical application. Chemical Society Reviews 46, 6570-6599.
Sreedhar, A., Noh, J.-S., 2021. Recent advances in partially and completely derived 2D Ti3C2 MXene based TiO2 nanocomposites towards photocatalytic applications: A review. Solar Energy 222, 48-73.
Srimuk, P., Kaasik, F., Krüner, B., Tolosa, A., Fleischmann, S., Jäckel, N., Tekeli, M.C., Aslan, M., Suss, M.E., Presser, V., 2016. MXene as a novel intercalation-type pseudocapacitive cathode and anode for capacitive deionization. Journal of Materials Chemistry A 4, 18265-18271.
Srivastava, N.K., Majumder, C.B., 2008. Novel biofiltration methods for the treatment of heavy metals from industrial wastewater. Journal of Hazardous Materials 151, 1-8.
Sun, Y., Xu, D., Li, S., Cui, L., Zhuang, Y., Xing, W., Jing, W., 2021. Assembly of multidimensional MXene-carbon nanotube ultrathin membranes with an enhanced anti-swelling property for water purification. Journal of Membrane Science 623, 119075.
Sun, Z.M., 2011. Progress in research and development on MAX phases: a family of layered ternary compounds. International Materials Reviews 56, 143-166.
Thakur, S., Sharma, B., Verma, A., Chaudhary, J., Tamulevicius, S., Thakur, V.K., 2018. Recent progress in sodium alginate based sustainable hydrogels for environmental applications. Journal of Cleaner Production 198, 143–159.
Thakur, S., Verma, A., Kumar, V., Jin Yang, X., Krishnamurthy, S., Coulon, F., Thakur, V.K., 2022. Cellulosic biomass-based sustainable hydrogels for wastewater remediation: Chemistry and prospective. Fuel 309, 122114.
Thakur, V.K., Thakur, M.K., 2015. Recent advances in green hydrogels from lignin: a review. International Journal of Biological Macromolecules 72, 834–847.
Thakur, V.K., Thakur, M.K., 2014. Recent Advances in Graft Copolymerization and Applications of Chitosan: A Review. ACS Sustainable Chem. Eng. 2, 2637–2652.
Thakur, V.K., Voicu, S.I., 2016. Recent advances in cellulose and chitosan based membranes for water purification: A concise review. Carbohydrate Polymers 146, 148–165.
Tunesi, M.M., Soomro, R.A., Han, X., Zhu, Q., Wei, Y., Xu, B., 2021. Application of MXenes in environmental remediation technologies. Nano Convergence 8, 5.
Umapathi, R., Sonwal, S., Lee, M.J., Mohana Rani, G., Lee, E.-S., Jeon, T.-J., Kang, S.-M., Oh, M.-H., Huh, Y.S., 2021. Colorimetric based on-site sensing strategies for the rapid detection of pesticides in agricultural foods: New horizons, perspectives, and challenges. Coordination Chemistry Reviews 446, 214061.

Urbankowski, P., Anasori, B., Makaryan, T., Er, D., Kota, S., Walsh, P.L., Zhao, M., Shenoy, V.B., Barsoum, M.W., Gogotsi, Y., 2016. Synthesis of two-dimensional titanium nitride Ti4N3 (MXene). Nanoscale 8, 11385-11391.
Usmani, Z., Sharma, M., Awasthi, A.K., Sivakumar, N., Lukk, T., Pecoraro, L., Thakur, V.K., Roberts, D., Newbold, J., Gupta, V.K., 2020. Bioprocessing of waste biomass for sustainable product development and minimizing environmental impact. Bioresource Technology 124548.
VahidMohammadi, A., Kayali, E., Orangi, J., Beidaghi, M., 2019. Techniques for MXene Delamination into Single-Layer Flakes. in: Anasori, B., Gogotsi, Y. (Eds.). 2D Metal Carbides and Nitrides (MXenes): Structure, Properties and Applications. Springer International Publishing, Cham, pp. 177-195.
Verma, A., Thakur, S., Mamba, G., Prateek, Gupta, R.K., Thakur, P., Thakur, V.K., 2020. Graphite modified sodium alginate hydrogel composite for efficient removal of malachite green dye. International Journal of Biological Macromolecules 148, 1130–1139.
Wang, H., Wu, Y., Xiao, T., Yuan, X., Zeng, G., Tu, W., Wu, S., Lee, H.Y., Tan, Y.Z., Chew, J.W., 2018. Formation of quasi-core-shell In2S3/anatase TiO2@metallic Ti3C2Tx hybrids with favorable charge transfer channels for excellent visible-light-photocatalytic performance. Applied Catalysis B: Environmental 233, 213-225.
Wang, H., Zhang, J., Wu, Y., Huang, H., Jiang, Q., 2017. Achieving high-rate capacitance of multi-layer titanium carbide (MXene) by liquid-phase exfoliation through Li-intercalation. Electrochemistry Communications 81, 48-51.
Wang, H., Zhang, J., Wu, Y., Huang, H., Li, G., Zhang, X., Wang, Z., 2016. Surface modified MXene Ti3C2 multilayers by aryl diazonium salts leading to large-scale delamination. Applied Surface Science 384, 287-293.
Wang, L., Xu, Z., Fu, D., Zhang, G., 2021. Challenging MXene-based Nanomaterials and Composite Membranes for Water Treatment. Current Analytical Chemistry 17, 731-736.
Wang, X., Kajiyama, S., Iinuma, H., Hosono, E., Oro, S., Moriguchi, I., Okubo, M., Yamada, A., 2015. Pseudocapacitance of MXene nanosheets for high-power sodium-ion hybrid capacitors. Nature Communications 6, 6544.
Wei, S., Xie, Y., Xing, Y., Wang, L., Ye, H., Xiong, X., Wang, S., Han, K., 2019. Two-dimensional graphene Oxide/MXene composite lamellar membranes for efficient solvent permeation and molecular separation. Journal of Membrane Science 582, 414-422.
Wu, Y., Pang, H., Liu, Y., Wang, X., Yu, S., Fu, D., Chen, J., Wang, X., 2019. Environmental remediation of heavy metal ions by novel-nanomaterials: A review. Environmental Pollution 246, 608-620.
Xiao, Y., Hwang, J.-Y., Sun, Y.-K., 2016. Transition metal carbide-based materials: synthesis and applications in electrochemical energy storage. Journal of Materials Chemistry A 4, 10379-10393.
Xie, X., Chen, C., Zhang, N., Tang, Z.-R., Jiang, J., Xu, Y.-J., 2019. Microstructure and surface control of MXene films for water purification. Nature Sustainability 2, 856-862.
Xu, B., Gogotsi, Y., 2020. MXenes: From Discovery to Applications. Advanced Functional Materials 30, 2007011.
Xu, C., Wang, L., Liu, Z., Chen, L., Guo, J., Kang, N., Ma, X.-L., Cheng, H.-M., Ren, W., 2015. Large-area high-quality 2D ultrathin Mo2C superconducting crystals. Nature Materials 14, 1135-1141.
Xu, J., Shim, J., Park, J.-H., Lee, S., 2016. MXene Electrode for the Integration of WSe2 and MoS2 Field Effect Transistors. Advanced Functional Materials 26, 5328-5334.
Xu, Z., Sun, Y., Zhuang, Y., Jing, W., Ye, H., Cui, Z., 2018. Assembly of 2D MXene nanosheets and TiO2 nanoparticles for fabricating mesoporous TiO2-MXene membranes. Journal of Membrane Science 564, 35-43.

Yang, J., Bao, W., Jaumaux, P., Zhang, S., Wang, C., Wang, G., 2019. MXene-Based Composites: Synthesis and Applications in Rechargeable Batteries and Supercapacitors. Advanced Materials Interfaces 6, 1802004.
Yang, K., Feng, L., Shi, X., Liu, Z., 2013. Nano-graphene in biomedicine: theranostic applications. Chemical Society Reviews 42, 530-547.
Yang, Q., Su, Y., Chi, C., Cherian, C.T., Huang, K., Kravets, V.G., Wang, F.C., Zhang, J.C., Pratt, A., Grigorenko, A.N., Guinea, F., Geim, A.K., Nair, R.R., 2017. Ultrathin graphene-based membrane with precise molecular sieving and ultrafast solvent permeation. Nature Materials 16, 1198-1202.
Yu, H., Wang, Y., Jing, Y., Ma, J., Du, C.-F., Yan, Q., 2019. Surface Modified MXene-Based Nanocomposites for Electrochemical Energy Conversion and Storage. Small 15, 1901503.
Zeng, G., Lin, Q., Wei, K., Liu, Y., Zheng, S., Zhan, Y., He, S., Patra, T., Chiao, Y.-H., 2021. High-performing composite membrane based on dopamine-functionalized graphene oxide incorporated two-dimensional MXene nanosheets for water purification. J Mater Sci 56, 6814-6829.
Zeng, Z., Yan, Y., Chen, J., Zan, P., Tian, Q., Chen, P., 2019. Boosting the Photocatalytic Ability of Cu2O Nanowires for CO2 Conversion by MXene Quantum Dots. Advanced Functional Materials 29, 1806500.
Zha, X.-H., Luo, K., Li, Q., Huang, Q., He, J., Wen, X., Du, S., 2015. Role of the surface effect on the structural, electronic and mechanical properties of the carbide MXenes. EPL (Europhysics Letters) 111, 26007.
Zhang, H., Li, M., Cao, J., Tang, Q., Kang, P., Zhu, C., Ma, M., 2018a. 2D a-Fe2O3 doped Ti3C2 MXene composite with enhanced visible light photocatalytic activity for degradation of Rhodamine B. Ceramics International 44, 19958-19962.
Zhang, S., Bilal, M., Adeel, M., Barceló, D., Iqbal, H.M.N., 2021. MXene-based designer nanomaterials and their exploitation to mitigate hazardous pollutants from environmental matrices. Chemosphere 283, 131293.
Zhang, T., Pan, L., Tang, H., Du, F., Guo, Y., Qiu, T., Yang, J., 2017. Synthesis of two-dimensional Ti3C2Tx MXene using HCl+LiF etchant: Enhanced exfoliation and delamination. Journal of Alloys and Compounds 695, 818-826.
Zhang, X., Xue, M., Yang, X., Wang, Z., Luo, G., Huang, Z., Sui, X., Li, C., 2015. Preparation and tribological properties of Ti3C2(OH)2 nanosheets as additives in base oil. RSC Advances 5, 2762-2767.
Zhang, X., Zhang, Z., Zhou, Z., 2018b. MXene-based materials for electrochemical energy storage. Journal of Energy Chemistry 27, 73-85.
Zhang, Y.-J., Lan, J.-H., Wang, L., Wu, Q.-Y., Wang, C.-Z., Bo, T., Chai, Z.-F., Shi, W.-Q., 2016. Adsorption of uranyl species on hydroxylated titanium carbide nanosheet: A first-principles study. Journal of Hazardous Materials 308, 402-410.
Zhao, Y., Wang, C.J., Gao, W., Li, B., Wang, Q., Zheng, L., Wei, M., Evans, D.G., Duan, X., O'Hare, D., 2013. Synthesis and antimicrobial activity of ZnTi–layered double hydroxide nanosheets. Journal of Materials Chemistry B 1, 5988-5994.
Zhou, W., Zhu, J., Wang, F., Cao, M., Zhao, T., 2017. One-step synthesis of Ceria/Ti3C2 nanocomposites with enhanced photocatalytic activity. Materials Letters 206, 237-240.
Zhu, C., Zeng, Z., Li, H., Li, F., Fan, C., Zhang, H., 2013. Single-Layer MoS2-Based Nanoprobes for Homogeneous Detection of Biomolecules. Journal of the American Chemical Society 135, 5998-6001.
Zhu, Q., Li, J., Simon, P., Xu, B., 2021. Two-dimensional MXenes for electrochemical capacitor applications: Progress, challenges and perspectives. Energy Storage Materials 35, 630-660.

Zou, G., Guo, J., Peng, Q., Zhou, A., Zhang, Q., Liu, B., 2016. Synthesis of urchin-like rutile titania carbon nanocomposites by iron-facilitated phase transformation of MXene for environmental remediation. Journal of Materials Chemistry A 4, 489-499.

Highlights:

- MXene-based nanomaterials (MBNs) for hazardous pollutants degradation.
- MXenes-based nanomaterials as nano-adsorbents to refine environmentally hazardous pollutants.
- Novel synthesis route, characteristics, and applications of MXenes-based nanomaterials.
- Recent challenges and prospects of MXene-based nanomaterials are highlighted.

Declaration of interests

☒ The authors declare that they have no known competing financial interests or personal relationships that could have appeared to influence the work reported in this paper.

☐The authors declare the following financial interests/personal relationships which may be considered as potential competing interests: